Mammalian Atg8 proteins regulate lysosome and autolysosome biogenesis through SNAREs

Yuexi Gu[1,2], Yakubu Princely Abudu[3], Suresh Kumar[1,2], Bhawana Bissa[1,2], Seong Won Choi[2], Jingyue Jia[1,2], Michael Lazarou[4], Eeva-Liisa Eskelinen[5], Terje Johansen[3], and Vojo Deretic[1,2]

[1] Autophagy, Inflammation and Metabolism (AIM) Center of Biomedical Research Excellence, University of New Mexico Health Sciences Center

[2] Department of Molecular Genetics and Microbiology, University of New Mexico Health Sciences Center

915 Camino de Salud, NE, Albuquerque, NM 87131, USA

[3] Molecular Cancer Research Group, Institute of Medical Biology, University of Tromsø-The Arctic University of Norway, 9037 Tromsø, Norway

[4] Department of Biochemistry and Molecular Biology, Biomedicine Discovery Institute, Monash University, Melbourne, Australia

[5] Institute of Biomedicine, University of Turku, Kiinamyllynkatu 10, Turku 20520, Finland

ABSTRACT

Mammalian homologs of the yeast Atg8 protein (mAtg8s) are important in autophagy, but their exact mode of action remains to be defined. Recently, syntaxin 17 (Stx17), a SNARE with major roles in autophagy, was shown to bind mAtg8s. Here we broadened the analysis of potential mAtg8-SNARE interactions and identified LC3-interacting regions (LIRs) in several SNAREs. Syntaxin 16 (Stx16), and its cognate SNARE partners all have LIR motifs and bind mAtg8s. A knockout in *STX16* caused defects in lysosome biogenesis whereas a double *STX16* and *STX17* knockout completely blocked autophagic flux and decreased mitophagy, pexophagy, xenophagy, and ribophagy. Mechanistic analyses revealed that mAtg8s and Stx16 maintained several aspects of lysosomal compartments including their functionality as platforms for active mTOR. These findings reveal a broad direct interaction of mAtg8s with SNAREs with impact on membrane remodeling in eukaryotic cells and expand the roles of mAtg8s to lysosome biogenesis.

INTRODUCTION

The autophagy pathway, controlled by a conserved set of *ATG* genes (Levine & Kroemer, 2019, Mizushima et al., 2011), is a cytoplasmic homeostatic process at an interface between quality control and metabolism. This pathway can be activated by metabolic and stress inputs (Garcia & Shaw, 2017, Marino et al., 2014, Noda & Ohsumi, 1998, Saxton & Sabatini, 2017, Scott et al., 2004) or triggered by cargo recognition leading to *in situ* assembly of ATG factors via receptor-regulators (Kimura et al., 2016, Lazarou et al., 2015, Mandell et al., 2014). Autophagy can be bulk or selective (Birgisdottir et al., 2013, Randow & Youle, 2014, Stolz et al., 2014), whereas the multiple biological outputs of autophagy depend on its completion and the type of termination of the autophagic pathway, e.g. degradation or secretion (Levine & Kroemer, 2019, Ponpuak et al., 2015). Bulk autophagy, whereby portions of the cytoplasm of heterogeneous composition are sequestered, occurs during starvation, and can be quantified by imaging (An & Harper, 2018) or biochemically (Engedal & Seglen, 2016, Seglen et al., 2015) by following sequestration of the cytosolic enzyme LDH, or ultrastructurally by enumerating partially degraded electron-dense ribosomes (Eskelinen, 2008, Tanaka et al., 2000). Autophagy can be selectively guided to specific cargo via a number of sequestosome 1/p62-like receptors (SLRs) (Birgisdottir et al., 2013, Bjorkoy et al., 2005, Stolz et al., 2014) or other classes of receptors besides SLRs (Kimura et al., 2016, Levine & Kroemer, 2019). Autophagy machinery is often recruited to damaged or dysfunctional targets after they are marked for autophagic degradation by ubiquitin and galectin tags that in turn are recognized by cytosolic autophagic receptors such as SLRs (Randow & Youle, 2014, Stolz et al., 2014). Autophagy apparatus can also be directly recruited via receptors resident to organelles if they become exposed following organellar membrane damage or depolarization, or are modified downstream of physiological or developmental signals (Bhujabal et al., 2017, Liu et al., 2012, Sandoval et al., 2008, Wei et al., 2017, Wild et al., 2011).

Degradative autophagy terminates in fusion of autophagosomes with lysosomes whereby the sequestered cargo is degraded. Examples of selective degradative autophagy include autophagy of mitochondria (mitophagy), peroxisomes (pexophagy), intracellular microbes (xenophagy), ribosomes (ribophagy), protein aggregates (aggrephagy), specific intracellular multiprotein complexes (precision autophagy) (An & Harper, 2018, Birgisdottir et al., 2013, Kimura et al., 2016, Randow & Youle, 2014). Given the diversity of cargo, complexity of the protein components and membrane compartments engaged, as well as the exquisite responsiveness to a variety of cargo-triggers (e.g. damaged organelles, aggregates) and stress conditions (e.g. starvation, hypoxia), autophagy is controlled by a collection of subsystems that have to come together in a modular fashion and cooperate in the initiation and execution of autophagy (Mizushima et al., 2011). These include: (i) formation of a complex between the ULK1 kinase, FIP200, ATG13 and ATG101, transducing mTOR inhibition

(Ganley et al., 2009, Hosokawa et al., 2009, Jung et al., 2009) and AMPK activation (Kim et al., 2011) to induce autophagy; (ii) generation of PI3P by the ATG14-endowed Class III PI3-Kinase Complex VPS34 (Baskaran et al., 2014, Chang et al., 2019, Petiot et al., 2000) that includes Beclin 1 (He & Levine, 2010), which can also be modified by AMPK to specifically activate the ATG14 form of VPS34 (Kim et al., 2013); (iii) the ubiquitin-like conjugation system with ATG5-ATG12/ATG16L1 (Mizushima et al., 1998a, Mizushima et al., 1998b) acting as an E3 ligase to lipidate mammalian homologs of yeast Atg8 (mAtg8s), some of which like LC3B have become key markers for autophagosomal membranes (Kabeya et al., 2000); (iv) the only integral membrane ATG protein, ATG9, and the ATG2-WIPI protein complexes, of still unknown but essential functions (Bakula et al., 2017, Velikkakath et al., 2012, Young et al., 2006). These modules are for the most part interconnected, with FIP200 physically bridging via ATG16L1 the ULK1/2 complex with the mAtg8s conjugation system (Fujita et al., 2013, Gammoh et al., 2013, Nishimura et al., 2013), ATG16L1 and WIPI directly interacting (Dooley et al., 2014), ATG13 connecting the ULK1/2 complex with VPS34 via ATG13's HORMA domain binding to ATG14 of the VPS34 complex (Jao et al., 2013, Park et al., 2016), and PI3P, the product of VPS34 (Petiot et al., 2000), being detected on membranes by WIPIs (Bakula et al., 2017).

In yeast, a component of the above systems morphologically equated with autophagy is Atg8, with its appearance as a single punctum defining the pre-autophagosomal structure (Kirisako et al., 1999). In mammals, this function is spread over a set of six mAtg8s (Mizushima et al., 2011, Weidberg et al., 2010), LC3A,B,C, GABARAP, -L1, and -L2. Although it is generally accepted that mAtg8s are important for autophagy, and that mAtg8 lipidation and puncta formation herald autophagy induction and isolation membrane formation, the core function of mAtg8s and possibly a direct role in autophagosomal membrane remodeling remains to be defined. Several models, including a direct role of Atg8/mAtg8s in catalyzing membrane fusion (Nakatogawa et al., 2007, Weidberg et al., 2011, Weidberg et al., 2010) have been considered but later challenged (Nair et al., 2011). Nevertheless, many of the cargos, selective autophagy receptors, and regulatory components (ULK, ATG13, FIP200, ATG14, Beclin 1, VPS34, ATG4) contain LC3-interacting regions (LIRs) and can either recruit cargo (Birgisdottir et al., 2013, Bjorkoy et al., 2005) or organize core autophagy machinery (Alemu et al., 2012, Birgisdottir et al., 2019, Skytte Rasmussen et al., 2017). Furthermore, recent studies show that even in the complete absence of mAtg8s, autophagosome formation proceeds, albeit with a lower sequestration volume, and that mAtg8s are important for autolysosomal formation (Nguyen et al., 2016a). In keeping with the latter findings, depletion of components participating in mAtg8 conjugation delays autophagic flux progression (Tsuboyama et al., 2016). It remains to be understood precisely how mAtg8s control membrane trafficking and remodeling during phagophore formation and elongation (Xie et al., 2008) and during autophagosome-lysosome fusion (Nguyen et al., 2016a, Weidberg et al., 2010).

Degradative aspects of autophagy depend on autophagosomes fusion with organelles of the endolysosomal system, often referred to as autophagic flux or autophagosome-lysosome fusion (Klionsky et al., 2016, Tanaka et al., 2000). Much of the intracellular membrane trafficking and fusion processes are catalyzed by SNARE proteins, which ensure compartment/organelle specificity through pairing of cognate Qa-, Qb-, Qc- and R-SNARE partners (Jahn & Scheller, 2006). SNAREs are often found in compartments where they function but also transit through other membranes, and thus their fusion activities are tightly regulated by tethers, SM (Sec1/Munc18) proteins, Rabs, and additional factors that modulate their recruitment, activation, cycles of reuse, etc., (Hong & Lev, 2014). In the context of autophagy, SNAREs have been studied at different stages along the autophagy pathway (Itakura et al., 2012, Kimura et al., 2017, Moreau et al., 2013, Nair et al., 2011). At the autophagosome-lysosome fusion stage, an initially identified SNARE was the Qa-SNARE Stx17, forming complexes with Qbc-SNARE SNAP29 and R-SNARE VAMP8 (Diao et al., 2015, Guo et al., 2014, Itakura et al., 2012, Takats et al., 2013, Wang et al., 2016). Recent studies have indicated that additional SNAREs may be required or even be dominant in this process (Matsui et al., 2018, Takats et al., 2018). Thus, redundant, complementary or synergistic SNARE-driven fusion and regulatory events may be at work during auto-lysosomal fusion. We have recently shown that Stx17 interacts via its LIR motif with mAtg8s, which functions in Stx17's recruitment to autophagosomes (Kumar et al., 2018), and that TBK1-phosphorylated Stx17 plays a role in autophagy initiation (Kumar & al., 2019), in keeping with studies by others (Arasaki et al., 2018, Arasaki et al., 2015, Hamasaki et al., 2013). Thus, Stx17 contributes to the autophagy pathway at several stages from initiation to maturation.

A report of direct interaction between mAtg8s and Stx17 (Kumar et al., 2018) has set an unanticipated precedent, and here we explored whether there is a broader range of interactions between mAtg8s and mammalian SNAREs. Using bioinformatics and biochemical approaches, we found additional candidate SNAREs with LIR motifs that bind mAtg8s. Among the candidates, we focused on a cognate set of SNAREs, Stx16, Vti1a and Stx6, previously implicated in retrograde transport between endosomes and the *trans*-Golgi network (TGN). Through mutational and functional analyses, we found that Stx16 acts synergistically with Stx17 and is important for diverse types of autophagy, including mitophagy, pexophagy, ribophagy, and elimination of intracellular *Mycobacterium tuberculosis*. We have further found that Stx16 is important for cellular lysosomal content and function, and that mAtg8s modulate Stx16 localization on endolysosomal organelles. This uncovers a mechanism different from the previous views of how mAtg8s help grow autophagosomal and complete autolysosomal membranes. We conclude that mAtg8s control autophagy at least in part by directly binding to SNARE proteins engaged in the biogenesis of the endolysosomal and autolysosomal organelles.

RESULTS

A subset of SNAREs including syntaxin 16 contain LC3-interacting regions

Previous studies have indicated that at least one SNARE involved in autophagy, Stx17, harbors a LIR motif that affects its distribution (Kumar et al., 2018). Here we carried out a broader analysis of all SNAREs for presence of putative LIR motifs using bioinformatics and conventional LIR motif consensus (Birgisdottir et al., 2013) followed up by biochemical assays (Fig. 1A and Appendix Table S1). We tested a subset of SNAREs containing putative LIRs in a screen with peptide arrays for binding to GST-GABARAP as a representative mAtg8 (Fig. 1A). Several SNAREs showed positive signals with GST-GABARAP in peptide arrays. These included only one R-SNARE, VAMP7, and mostly Qa-, Qb-, and Qc-SNAREs acting in different cellular compartments (Jahn & Scheller, 2006): Stx17, included as a positive control (Kumar et al., 2018) and already implicated in autophagy (Itakura et al., 2012), Stx18 acting in the ER (Hatsuzawa et al., 2000), GOSR1 functioning in the Golgi (Mallard et al., 2002, Subramaniam et al., 1996), Stx3 and Stx4 on plasma membrane (Low et al., 1996), Stx19 with no transmembrane domain and partitioning between cytosol and membranes (Wang et al., 2006), and Stx16, Stx6 and Vti1a, all acting in trafficking between endosomal compartments and TGN (Jahn & Scheller, 2006, Malsam & Söllner, 2011) (Fig. 1B and Fig. EV1A). Thus, a number of SNAREs may be binding partners for mAtg8s indicating a previously unappreciated potential for broader intersections between mAtg8 and SNARE systems.

Syntaxin 16 directly binds mAtg8s through its LIR motif

From the panel of SNAREs showing positive signals with GST-GABARAP in peptide arrays, we focused on a set of three cognate SNAREs, Stx16, Vti1a, and Stx6, known to form a complex (Malsam & Söllner, 2011). Co-immunoprecipitation (Co-IP) analyses of over-expressed fusion proteins confirmed that Stx16, Vti1a and Stx6 interact with LC3B and GABARAP (Fig. 1C). Co-IP analyses of endogenous proteins in HeLa and U2OS cells confirmed interactions between LC3 and Stx16 and Vti1a (Fig. EV1B). In GST pull-down assays with all 6 mAtg8 proteins, Stx16 showed a positive binding signal with LC3C, GABARAP, and GABARAPL1 (Fig. 1D). The peptide array binding results pointed to the ^{219}LVLV^{222} residues in Stx16 (Fig. 1B), which resembled both the LC3C-preferring LIR of NDP52 (ILVV) (von Muhlinen et al., 2012) and the GABARAP-interaction motifs with important Val residues in second and fourth positions of the core LIR motif (Rogov et al., 2017). This motif was found in the linker region between the Habc and SNARE domains of Stx16 matching the requirement to be outside of known structured regions (Popelka & Klionsky, 2015). When we mutated L-219 and V-222 in the predicted (albeit atypical) LIR motif (^{219}LVLV^{222} mutated to ^{219}AVLA^{222}) of Stx16, this reduced Stx16 binding to LC3C and GABARAP (Fig. 1E). Additionally, we changed both Val residues within the ^{219}LVLV^{222} motif to Ala, and the resulting Stx16 variant showed

reduction in binding to LC3C and GABARAP comparable to the ^{219}AVLA^{222} mutant in GST pull-down experiments (Fig. 1F). Finally, when we mutated all 4 residues within the ^{219}LVLV^{222} motif, the association between Stx16 and LC3C or GABARAP was completely abolished (Fig. 1F).

Complementary to the above experiments with LIR mutations, we tested whether the previously defined LIR-docking site (LDS) in GABARAP (Behrends et al., 2010, Birgisdottir et al., 2013) was responsible for binding to Stx16. Two conserved hydrophobic pockets (HP1 and HP2) are known to define the LIR-docking site of GABARAP (Behrends et al., 2010). The Y49A mutation in the HP1 pocket of GABARAP reduced its interaction with Stx16, whereas the complete LDS mutant (double HP1 and HP2 Y49A/F104A mutation) abrogated GABARAP's binding to Stx16 in GST pull-down assays (Fig. 1G). Thus, GABARAP and Stx16 interaction depends on the canonical LDS motif in GABARAP.

Syntaxin 16 is required for efficient autophagy flux in response to starvation

Stx17 has been implicated in mammalian autophagosome-lysosome fusion (Itakura et al., 2012). However, additional SNAREs have now been shown to contribute to this process (Matsui et al., 2018), but relative contributions remain to be fully defined. We generated CRISPR/Cas9-mediated *STX17* knockout (KO) in different cell lines (HeLa and Huh7; Fig. EV2A and B) and analyzed autophagy flux by monitoring LC3-II levels (Fig. 2A and B; Fig. EV2C and D). In *STX17*^{KO} HeLa cells, the autophagic flux continued at almost the same rates as in wild type (WT) control cells, as shown by slight increase of LC3-II levels upon starvation (Fig. 2A). A similar effect was observed in hepatocellular carcinoma Huh7 *STX17*^{KO} cells, which in general displayed faster LC3-II flux (Fig. EV2C and D). Knocking out Stx17 did not cause any significant change in the levels of p62, an autophagic receptor that is degraded upon starvation (Bjorkoy et al., 2005) and is often used as readout of autophagic flux (Klionsky et al., 2016) (Fig. 2A and Fig. EV2C).

When we knocked out *STX16* in HeLa cells, this too had no major effects on LC3-II flux (Fig. EV2A and B; Fig. 2C and D). However, when a double *STX16/STX17* knockout was generated (Fig. EV2B), the LC3 flux was completely abrogated, with LC3-II levels in starvation-induced cells accumulating at similar levels as in cells treated with bafilomycin A1 (Fig. 2C and D), usually considered as a complete blocker of autophagic flux (Klionsky et al., 2016). The LC3-II accumulation could be partially relieved by complementation of *STX16/STX17*^{DKO} cells transfected with FLAG-tagged WT Stx16 (Fig. EV2E). Given that this indicated a block in autolysosome production, we examined *STX16/STX17*^{DKO} cells using automated quantitative high-content microscopy (HCM) and tandem mCherry-EYFP-GABARAP, by monitoring and quantifying overlap between red (mCherry) and green (EYFP) fluorescence as another measure of autophagic

flux. The overlap between mCherry and EYFP was significantly increased in *STX16/STX17*^{DKO} cells compared to that in WT cells upon starvation in EBSS (Fig. EV2F and G). At the ultrastructural level, electron microscopy quantification of initial (AVi) vs. degradative (AVd) autophagic vacuoles (Eskelinen, 2008, Tanaka et al., 2000) also indicated accumulation of AVi vesicles (Fig. 2E and F). In conclusion, absence of either Stx16 or Stx17 alone cannot block completion of the autophagy pathway, but when both are ablated, this prevents progression to autolysosomes.

Syntaxin 16 and syntaxin 17 are required for completion of diverse selective autophagy processes

Mitophagy is a very well-studied process of selective autophagy and is often used as an example to study elimination of defunct organelles (Youle & Narendra, 2011). To further characterize effects of *STX16*/*STX17* double knockout, we employed HCM quantification of mitochondrial DNA (mtDNA) as a measure of cellular mitochondrial content often used in mitophagy studies (Lazarou et al., 2015, Nguyen et al., 2016b). We generated *STX16*/*STX17* DKO in HeLa cells stably expressing YFP-Parkin (Lazarou et al., 2015) (Fig. EV3A). We then stressed mitochondria using two different depolarizing agents: CCCP or oligomycin A + antimycin A (OA), and quantified Parkin-dependent mitophagy in *STX16*/*STX17*^{DKO} HeLa/YFP-Parkin cells. In wild type cells, CCCP or OA caused a major reduction in mtDNA (Fig. 3A and B). Loss of Stx16 and Stx17 caused significant reduction in mitophagy (Fig. 3A and B). Clearly, additional processes were also involved as *STX16*/*STX17*^{DKO} HeLa/YFP-Parkin cells still eliminated mitochondria probably through additional mechanisms (Nguyen et al., 2016a). Previous studies indicated that Stx17 is not important for mitophagy (Nguyen et al., 2016b). Nevertheless, a loss of Stx16 in the *STX17*^{KO} background affected mitophagy significantly.

Pexophagy is another classical example of selective autophagy (Gatica et al., 2018, Manjithaya et al., 2010). We monitored pexophagy in cells treated with H_2O_2 (Zhang et al., 2015) using liver cell line Huh7, which expresses wild type LKB1 that can activate AMPK (Tan et al., 2018) (Fig. EV3B). We monitored pexophagy by quantifying levels of PEX14 and PMP70 (Zhang et al., 2015) proteins, and detected decrease in these peroxisomal constituents over a period of 6 hours of exposure to H_2O_2 (Fig. 3C). In cells lacking both Stx16 and Stx17, this reduction in peroxisomal protein levels was abrogate (Fig. 3C and D). Thus, *STX16*/*STX17* DKO significantly inhibited pexophagy.

Autophagic defense against intracellular microbes, such as *Mycobacterium tuberculosis* (*Mtb*) (Gutierrez et al., 2004), sometimes referred to as xenophagy, is considered to be another form of selective autophagy. We tested the survival of *M. tuberculosis* in macrophage-like cell line THP1 and compared the effects of *Mtb* killing in WT, single *STX16*^{KO} or *STX17*^{KO} and *STX16/STX17*^{DKO} cells (Fig. EV3C). As previously reported (Gutierrez et al., 2004), induction of autophagy by

starvation reduced survival of *Mtb* in WT THP1 cells (Fig. 3E). However, this effect was lost in *STX16*^{KO} THP1 cells (Fig. 3E; Fig. EV3C). Further analyses of combination CRISPR KO mutants of *STX17* alone, previously reported in THP1 cells to play a role in control of intracellular *Mtb* (Kumar et al., 2018), or both *STX16* and *STX17*, showed no further additive effects between Stx16 and Stx17 (Fig. 3E).

Taken together, these data indicate that *STX16*/*STX17* DKO significantly reduces mitochondrial (Lazarou et al., 2015), peroxisomal (Manjithaya et al., 2010), and bacterial (*Mtb*) (Gutierrez et al., 2004) clearance under conditions known to induce autophagy (Fig. 3F).

Keima-based ribophagy probes indicate a role of Stx16 in autophagic maturation

Keima fluorescent protein has become an important tool for detection of the arrival of autophagy substrates to autolysosomes (Katayama et al., 2011). In functional autolysosomes, despite being in a degradative compartment, Keima protein is stable but changes its spectral properties (illustrated in Fig. 4A) from maximum excitation wavelength at 440 nm in neutral pH to 586 nm in acidic pH, with emission remaining constant at 620 nm (Violot et al., 2009). These shifts can be monitored using 440 nm and 560 nm excitation filters and emission at 620 nm in an HCM Cellomics system (see Methods). We applied Keima to monitor ribophagy (An & Harper, 2018), and generated *STX16*/*STX17* DKO using CRISPR/Cas9 (Fig. 4B) in HEK293 cells stably expressing RPS3-Keima (fusion between 40S ribosomal protein S3 and mKeima) protein (An & Harper, 2018). RPS3-Keima was diffuse cytoplasmic in untreated cells. Under starvation conditions, we examined ribophagy as previously reported (An & Harper, 2018), by monitoring progression of RPS3-Keima into acidic autolysosomal compartments via quantification of cytoplasmic puncta at 560 nm excitation and 620 emission wavelengths (Fig. 4C and D). The HEK293 *STX16*/*STX17*^{DKO} cells showed significantly fewer autolysosomal puncta originating from RPS3-Keima than in parental WT cells (Fig. 4C and D). An independent set of experiments was carried out with HCT116 cells stably expressing a fusion between 60S ribosomal protein L28 and mKeima (RPL28-Keima). We generated *STX16*/*STX17* DKO in these cells as well using CRISPR/Cas9 (Fig. 4B). Progression of ribophagy in HCT116 RPL28-Keima *STX16*/*STX17*^{DKO} cells was diminished relative to parental WT cells (Fig. 4E and F). Thus, the use of previously characterized Keima ribophagy probes (An & Harper, 2018) further confirmed the importance of having both Stx16 and Stx17 for autophagic cargos to arrive into acidified compartments, including during ribophagy.

Syntaxin 16 plays a role in lysosomal biogenesis

When we tested autophagy response by monitoring endogenous LC3 puncta, we found an increase in LC3 dots in *STX16* knockout cells (HeLa *STX16*^{KO}) relative

to WT cells, under basal conditions and in EBSS-starved cells (Fig. 5A and B). Next, we determined by HCM the overlap area between LC3 and LAMP2 profiles, and found that the overlap was strongly reduced in HeLa *STX16*^{KO} vs WT cells (Fig. 5A and C). When we quantified LAMP2 puncta/cell, we found that LAMP2^{+} puncta were diminished in HeLa *STX16*^{KO} cells (Fig. 5A and D). Thus, the appearance of reduced colocalization (overlap area by HCM) between LC3 and LAMP2 was not a result of fewer autolysosomes but was primarily due to the overall reduction of LAMP2^{+} organelles in *STX16*^{KO} cells (Fig. 5A and D), a phenotype that could be complemented by reintroducing WT Stx16 but less so with a LIR mutant of Stx16 (Appendix Fig. S1A and B). The reduction in cytoplasmic content of LAMP2^{+} organelles in HeLa *STX16*^{KO} cells was also seen by immunoblots, showing reduced total LAMP1 and LAMP2 protein levels in cells knocked out for Stx16 (Fig. 5E). This was further tested by generating *STX16* knockout in different cell lines (Fig. EV2A and B). As with different clones of HeLa *STX16*^{KO} cells, different single clones of Huh7 *STX16*^{KO} and osteosarcoma U2OS *STX16*^{KO} cells had reduced LAMP1 and LAMP2 protein levels (Fig. 5E). Thus, Stx16 is important for the maintenance of homeostatic LAMP levels. We also generated CRISPR knockouts for Stx6 and Vti1a, and found reduced levels of LAMP2 in *STX6*^{KO} and *VTI1A*^{KO} HeLa cells (Fig. 5F). Thus, Stx16 and its cognate Qb- and Qc-SNAREs affect cellular LAMP levels.

Prior ultrastructure studies have implicated HOPS component VPS41 in LAMP1 and LAMP2 transport from the TGN to late endosomal compartments (Pols et al., 2013). In *STX16*^{KO} HeLa cells, there was increased colocalization of detectable LAMP2 with the TGN marker TGN46, normalized for LAMP puncta in HCM quantifications (Fig. EV3D and E). We thus tested whether Stx16 and its cognate Qb- and Qc-SNAREs, Vti1a and Stx6 (both showing positivity in mAtg8 peptide binding arrays; Fig. 1A) interact with VPS41. Using FLAG-tagged Stx6 and Stx16 we detected VPS41 in FLAG immunoprecipitates (Fig. EV3F). We found VPS41 but not VPS33A (a component of the HOPS complex) in endogenous protein complexes with Stx6, and Vti1a (Appendix Fig. S1C). These observations suggest a connection of Stx16 (plus Vti1a and Stx6) to VPS41 and the transport of lysosomal proteins such as LAMP1 and LAMP2, previously proposed specifically for VPS41 and not other components of HOPS (Pols et al., 2013).

Starvation increases interactions of Stx16 with the lysosomal R-SNARE VAMP8

We found that Stx16 interacts with VAMP3 and VAMP4 (Fig. EV3F), consistent with the known literature regarding VAMP3 and VAMP4 as cognate R-SNAREs during retrograde transport from endosomes to TGN (Ganley et al., 2008, Mallard et al., 2002). However, upon starvation another R-SNARE, VAMP8, increased its presence in Stx16 complexes (Fig. EV3F). The lysosomal SNARE VAMP8 (Jahn & Scheller, 2006) has not been previously implicated in Stx16-dependent trafficking, and our findings suggest a new relationship detected only under

starvation conditions. Similarly, Stx6, a Qc-SNARE working together with Stx16, showed increased interactions with VAMP8 in starved cells (Fig. EV3F). Thus, similar relationship to VAMP8 was observed with both Stx16 and Stx6. We also noticed increased Stx6-VAMP3 interactions in starved cells (Fig. EV3F), and interpret this as an overall increase in trafficking between TGN and the lysosomal/endosomal pathway.

Stx16 affects mTOR regulation

Lysosomes are not only digestive organelles but also serve as a principal cytoplasmic location for active mTOR (Betz & Hall, 2013, Lawrence & Zoncu, 2019, Saxton & Sabatini, 2017). Given that we detected defects in LAMP1/2 levels and profiles (Fig. 5D and E) in *STX16*^{KO} cells, we wondered whether mTOR would be affected and serve as another reporter of the lysosomal status in this context. We tested mTOR activity by monitoring phosphorylation of its downstream targets, such as 4E-BP1 (Gingras et al., 1999), and ULK1^{S757}, with latter being a principal phospho-site for ULK1 and repression of autophagy by mTOR (Kim et al., 2011). Under resting conditions, no differences in mTOR activation status were observed in *STX16*^{KO} vs WT cells (Fig. 5G). Under starvation conditions, as expected, mTOR activity was reduced, but this reduction was much more pronounced in *STX16*^{KO} cells (Fig. 5G).

In resting cells, active mTOR forms cytoplasmic puncta and localizes to lysosomes (Betz & Hall, 2013, Saxton & Sabatini, 2017), but in starved cells mTOR is less punctate and translocates from lysosomes into the cytoplasm (Sancak et al., 2010). Under resting conditions (full medium), mTOR puncta (quantified by HCM) were not reduced in *STX16*^{KO} vs WT cells (Fig. 5H and I). One hour of starvation reduced mTOR puncta, as quantified by HCM (Fig. 5H and I), reflecting mTOR inactivation. This effect was more pronounced in *STX16*^{KO} cells relative to WT cells (Fig. 5H and I). When the cells were starved for 6 hours, a time point that coincided with mTOR persistent inactivation assessed by phosphorylation of its targets (Fig. 5G), we found an even stronger reduction in total mTOR puncta (Appendix Fig. S2A and B). Localization of mTOR to LAMP2^{+} profiles was reduced by starvation (examined at 6 h; Fig. EV4A and B), an effect that was more pronounced in *STX16*^{KO} relative to WT cells. Thus, Stx16 affects mTOR activation state, correlating with the role of Stx16 in cellular lysosomal status.

Stx16 is required for appropriate distribution of acidified compartments in the cell

Since *STX16* knockout resulted in reduced cellular content of LAMP1/2, which is in lysosomal and additional acidified endosomal compartments (Lippincott-Schwartz & Fambrough, 1987) (Cheng et al., 2018), we anticipated that the cells might have diminished content of acidified organelles. We used LysoTracker Red DND-99 (LTR) as a standard cell biological probe for acidification of intracellular

compartments (Wubbolts et al., 1996). Surprisingly, we found no change in total LTR fluorescence by number of profiles/cell or total area/cell (Fig. 6A and B) utilizing HCM (Cellomics) and comparing WT and *STX16*^{KO} HeLa cells under autophagy-inducing conditions (starvation). This was confirmed by total LysoTracker Green DND-26 (LTG) fluorescence and LTG puncta/cell using ImageStream flow cytometry (Amnis) in WT vs *STX16*^{KO} cells induced for autophagy (Appendix Fig. S3A–C). However, when we examined localization and morphology of LTR^{+} profiles in *STX16*^{KO} cells, under autophagy-inducing conditions when LTR^{+} organelles were strongly enhanced (relative to the resting conditions), we found that the LTR labeling redistributed from its usual presentation as cytoplasmic puncta into a compartment clustering in a perinuclear region colocalizing with the TGN marker TGN46 (Fig. 6C and D). To ensure that the Golgi apparatus was not perturbed, we re-examined the ultrastructural images in Fig. 2E, and found that the overall morphology of the Golgi stacks was similar in WT and mutant cells, but that the volume fraction of the Golgi compartment was increased (Fig. 6E), consistent with an increased retention of acidified compartments in the Golgi. Furthermore, TGN46 did not show major changes in distribution relative to the Golgi marker GM130 (Fig. EV4C and D) and relative to another factor in TGN-endolysosomal trafficking, mannose 6-phosphate receptor/M6PR (Fig. EV4E and F). Thus, the effects of Stx16's absence entail redistribution of acidified compartments, in keeping with a reduction in levels of the integral lysosomal membrane proteins LAMP1 and LAMP2.

Mammalian Atg8s regulate Stx16 localization to endosomal and lysosomal compartments

Since Stx16 is an mAtg8-binding SNARE (Fig. 1), we tested whether mAtg8s influenced Stx16 localization in the cell. We used the previously characterized triple LC3A,B,C knockout (Tri-LC3^{KO}), triple GABARAP, -L1, -L2 knockout (Tri-GBRP^{KO}), and all six mATG8s knockout (Hexa^{KO}) HeLa cells (Nguyen et al., 2016a) (Fig. EV5A). First, we tested LAMP1 and LAMP2 protein levels in Tri-LC3^{KO}, Tri-GBRP^{KO} and Hexa^{KO} cells. LAMP levels were not reduced under resting conditions in mAtg8 mutant cells by quantifying LAMP2^{+} organelles (HCM, number of puncta/cell and total area/cell) (Appendix Fig. S4A and B) as well as by Western blot analysis of LAMP1/2 proteins (Appendix Fig. S4C). We nevertheless observed a minor LAMP reduction, possibly reflecting "exhaustion" during long-term (8 h) starvation, in Tri-GBRP^{KO} and Hexa^{KO} cells (Appendix Fig. S4D). When we assessed localization of Stx16 to LAMP2 (lysosome) and LBPA (late endosome), we observed significantly reduced colocalizations between Stx16 and LAMP2 as well as Stx16 and LBPA by several HCM measures: (i) LAMP2-Stx16 overlap (Fig. 7A and B); and (ii) LBPA-Stx16 overlap (Fig. 7C; Appendix Fig. S5A). Comparing STX16 WT and its ^{219}LVLV^{222}, ^{219}AVLA^{222}, or LIR-4A mutants, the LIR mutants showed reduced localization to LAMP2 profiles when compared to WT (Fig. EV5B and C). Thus, mAtg8s and their binding site (LIR) on Stx16 play a role in placement of Stx16 on lysosomes.

Endogenous Co-IP analyses showed reduced interactions between components of the Stx16/Vti1a/Stx6 SNARE complex in Tri-GBRP^{KO} and Hexa^{KO} cells (Fig. EV5D), suggesting a regulatory role mAtg8s in SNARE complex assembly or stability. A lipidation status of mAtg8s may be of significance as well, since we observed reduced interactions between Stx6 and Stx16, Vti1a or VPS41 in *ATG3*^{KO} HeLa cells generated by CRISPR/Cas9 (Fig. EV5E); ATG3 is a key factor required for lipidation of mAtg8s (Mizushima et al., 2011). We next tested cellular acidified compartments by HCM and Amnis, and quantified effects of mAtg8 mutants. In Hexa^{KO} cells, the overall LTR^{+} profiles were reduced by HCM (Fig. 7D and E) and LTG^{+} profiles were reduced by ImageStream flow cytometry (Appendix Fig. S5B–D). mAtg8s also had an effect on mTOR inactivation in response to starvation, as evidenced by a more pronounced loss of phosphorylation of mTOR targets ULK1 (phospho-Ser757) and 4E-BP1 (phospho-Thr37/46) in Hexa^{KO} cells relative to WT HeLa cells (Fig. EV5F). In summary, albeit mAtg8s do not completely parallel Stx16 phenotype, they do have an effect on Stx16 distribution and mTOR inactivation. Additionally, mAtg8s show strong effects on acidified, LTR^{+} compartments in cells under autophagy inducing conditions. Thus, mAtg8s and Stx16 have partially overlapping effects on the endolysosomal system.

DISCUSSION

Here we uncovered a broad potential for interactions between the core autophagy components, mAtg8s, and the core membrane fusion system composed of SNAREs. The bioinformatics analyses and follow-up biochemical experiments indicate that mAtg8s and several SNAREs work together in membrane trafficking and organelle biogenesis. One subset of SNAREs interacting with mAtg8s, Stx16-Vti1a-Stx6, was examined in detail, and Stx16 was fully characterized for mAtg8 binding, as has been done for Stx17 (Kumar et al., 2018). This leads us to propose a model departing from the conventional views of how LC3 or other mAtg8s work in autophagy, suggesting a new mechanism of control of membrane trafficking/fusion through direct action of mAtg8s on SNARE molecules (Fig. 7F).

Our findings with Stx16 indicate a function for mAtg8s in the maintenance of lysosomal compartments (Fig. 7F), through binding directly and regulating SNAREs of the Stx16 complex, which leads up to autolysosome biogenesis. This amends the conventional view of mAtg8s expanding the autophagosomal membranes (Carlsson & Simonsen, 2015) and complements more recent views of mAtg8s working in the recruitment of various components of the autophagic apparatus. These include: (i) mAtg8 binding to autophagic receptors from the SLR (Birgisdottir et al., 2013, Rogov et al., 2014) and TRIM (Keown et al., 2018, Mandell et al., 2014) families of receptors; (ii) the ULK1-FIP200-ATG13 autophagy initiation complex (Alemu et al., 2012); (iii) a large number of ancillary components facilitating the autophagosome-lysosome fusion (Kriegenburg et al., 2018, McEwan et al., 2015, Olsvik et al., 2015, Wang et al., 2016); and (iv) non-autophagic roles of mAtg8s, such LAP (Sanjuan et al., 2007), LAP-like processes (Florey et al., 2015), MVB/exosome formation (Guo et al., 2017), and via binding to TECPR2 in the COPII-dependent ER export (Stadel et al., 2015).

Human cells have 6 mAtg8s, with proposed but not fully delineated specialized functions (Shpilka et al., 2011). Their role has been established in the recruitment of several important ancillary factors facilitating membrane fusion at the autophagosome-lysosome fusion stage of the autophagic pathway (Nakamura & Yoshimori, 2017). An early study has shown GABARAPL2/GATE-16 interaction with NSF enhancing its ATPase activity thus implicating it in activation of the Golgi SNARE GOS-28/GOSR1 (Sagiv et al., 2000), of consequence for post-mitotic Golgi reformation (Muller et al., 2002) and intra-Golgi transport (Sagiv et al., 2000). This is in keeping with the results of our screen of mAtg8-interacting SNAREs and is compatible with the concept of mAtg8s directly acting on SNAREs.

Stx16 and its cognate SNAREs have been shown to play a role in retrograde trafficking from endosomal compartments to TGN with two distinct pairings of Qa-, Qb-, and Qc-SNAREs: (i) Stx16, Vti1a, Stx10, required specifically for M6PR transport (we did not observe effects on M6PR relative to

TGN46 in our studies), which impacts trafficking of lysosomal hydrolases (Ganley et al., 2008); and (ii) Stx16, Vti1a, and Stx6, which is independent of the Stx10/M6PR pathway and controls trafficking to TGN of endocytosed incoming toxins bound to membrane glycoconjugates (Mallard et al., 2002). There is also a Stx16-independent retrograde pathway that instead depends on GOS-28/GOSR1 (Tai et al., 2004), another SNARE that incidentally binds mAtg8s (see Fig. 1A, 6th peptide array from the top). Of note, GOS-28/GOSR1 has been first described as a GATE-16-binding SNARE (Sagiv et al., 2000) with Golgi functions. Most of the prior studies with Stx16 complexes have been focused on retrograde trafficking to the TGN, and thus our observations could be due to perturbed retrograde membrane and cargo flow. However, our findings that Stx16 is in complexes with VPS41, previously implicated in anterograde transport of LAMP1/2 (Pols et al., 2013), and reduced abundance of LAMP1/2^{+} organelles in *STX16*^{KO} cells suggest that Stx16 defect blocks the prograde delivery of LAMP1/2 during lysosomal biogenesis.

Trafficking of various components that make up functional lysosomes is only partially understood (Bright et al., 2016, Luzio et al., 2000, Saftig & Klumperman, 2009) especially regarding anterograde pathways to lysosomes of integral membrane proteins such as LAMP1/2 and trafficking to and assembly at the lysosome of the V_1V_0 holoenzyme vacuolar H^+-ATPase (Saftig & Klumperman, 2009). Our findings suggest that Stx16 is responsible for LAMP1/2 trafficking to lysosomes with secondary consequences on the overall levels of LAMPs when this delivery is disrupted. It is likely that Stx16 does not affect vacuolar H^+-ATPase's ability to function but these acidified compartments may be displaced due to a lack of clearly defined lysosomal destination. Some of *STX16*^{KO} phenotypes (perturbation of acidified compartments) are echoed in mAtg8s null Hexa^{KO} cells, which show diminished overall content of acidified organelles. These phenomena can in part be explained by mAtg8s affecting Stx16 localization. Since Hexa^{KO} effects on acidification are more pronounced than the effects of *STX16*^{KO}, this indicates additional functions for mAtg8s, specifically in H^+-ATPase function. For example, it has recently been shown that LC3 affects ATP6V1E1 subunit of the V_1 domain of vacuolar H^+-ATPase (Guo et al., 2017). Although mAtg8s do not phenocopy in full the Stx16 phenotype, they do affect Stx16 distribution and mTOR activity. Thus, mAtg8s and Stx16 have only partially overlapping effects on the endolysosomal system most likely due to mAtg8 action exceeding the reach of the Stx16 function.

Since lysosomes are the location of active mTOR (Betz & Hall, 2013, Saxton & Sabatini, 2017), we used mTOR activity as another readout of Stx16 effects on the lysosomal function. Somewhat surprisingly, given the strong reduction of LAMP1/2 levels and diminished number of $LAMP^+$ organelles, *STX16*^{KO} did not show effects on basal mTOR activity. However, during starvation, which inactivates mTOR and triggers its translocation from the lysosomes, mTOR was inhibited far more prominently in *STX16*^{KO} cells and this was also reflected in fewer $mTOR^+$ cytoplasmic puncta. One interpretation is that the reduced LAMP1/2 content differentially affects subpopulations of lysosomes (Bright et al., 2016) and that the ones that are platforms for active mTOR are preferentially preserved/maintained. Nevertheless, upon stress and perturbance, inactivation of mTOR is more effective and more durable in *STX16*^{KO} cells. This could be a reflection of altered trigger thresholds dependent on diminished lysosomal sources of nutrients and/or difficulties in re-establishing nutrient equilibrium and mTOR activity. Alternatively, Stx16 may be important in transport to lysosomes of additional mTOR regulatory components important for its reactivation.

The Qa-SNARE Stx17 was first appreciated as a key SNARE in autophagosome-lysosome fusion (Diao et al., 2015, Guo et al., 2014, Itakura et al., 2012, Takats et al., 2013, Wang et al., 2016). Recent studies have uncovered the yeast SNARE, Ykt6, as important in autophagosome-vacuole/lysosome fusion in yeast (Bas et al., 2018, Gao et al., 2018), and that mammalian Ykt6 ortholog (Matsui et al., 2018, Takats et al., 2018) plays a potentially dominant (over Stx17) role in mammalian autophagosome-lysosome fusion. Whereas the exact mechanism of Ykt6 in maturation has not been agreed upon, with differences in proposed models (Matsui et al., 2018, Takats et al., 2018), it is worth noting that Ykt6 is also part of one of retrograde trafficking routes from endosomes to TGN that includes GOS-28/GOSR1 (Tai et al., 2004), an mAtg8-binding SNARE as discussed above. Nevertheless, our data here suggest that Stx17 still plays a very important role in autophagosomal flux, revealed in the requirement for a *STX16*/*STX17* double KO to block autophagic flux using the conventional and well accepted LC3 flux assay (Klionsky et al., 2008), and reflected in autophagic degradation of a diverse panel of substrates: mitochondria, peroxisomes, *M. tuberculosis*, and ribosomes.

Stx17 interacts via its LIR motif with mAtg8s, and this may play a role in its recruitment to autophagosomes as a prelude to fusion with the lysosomes (Kumar et al., 2018). However, Stx17's role in autophagy begins much earlier, during initiation (Arasaki et al., 2018, Arasaki et al., 2015, Hamasaki et al., 2013, Kumar & al., 2019) ensuring that once autophagosomes are formed they are enabled for fusion with endolysosomal compartments. The present screen for other SNAREs that bind mAtg8s yielded a number of candidates in addition to Stx16, such as Vti1a and Stx6, which partner with Stx16, and Stx3 and Stx4, SNAREs that are engaged in secretory autophagy (Kimura et al., 2017). This

prompts us to suggest that mAtg8s' function in autophagy should be reconsidered and some of its mechanistic principles revisited. We propose that mAtg8s act by reshaping overall membrane trafficking in the cell through direct interactions and effects on specific SNAREs and redirect membrane flow toward autophagy at its initiation and termination stages.

Materials and Methods

Antibodies and reagents

Antibodies: rabbit anti-LC3B (L7543, for WB), rabbit anti-STX17 (HPA001204), and mouse anti-FLAG (F1804, for WB and IP) were from Sigma-Aldrich; mouse anti-LC3 (M152-3, for WB and IP) and rabbit anti-LC3 (PM036, for IF) were from MBL International; mouse anti-p62 (#610833) and mouse anti-GM130 (#610823) were from BD Biosciences; rabbit anti-STX16 (NBP1-92467), rabbit anti-VAMP3 (NB300-510), rabbit anti-VAMP4 (NBP2-13512), rabbit anti-VPS33A (NBP2-20872) and rabbit anti-TGN46 (NBP1-49643) were from Novus Biologicals; mouse anti-STX6 (H00010228-M01, for WB and IP) was from Abnova; mouse anti-Vti1a (sc-136117), mouse anti-VAMP8 (sc-166820) mouse anti-ATG3 (sc-393660) and mouse anti-β-actin (sc-47778) were from Santa Cruz Biotechnology; rabbit anti-VPS41 (ab181078), rabbit anti-PEX14 (ab183885), rabbit anti-PMP70 (ab85550), rabbit anti-GFP (ab290) and rabbit anti-β-tubulin (ab18251) were from Abcam; rabbit anti-LAMP1 (D2D11) (#9091), Phospho-AMPKα (Thr172) (#2531), AMPKα (#2532), Phospho-ULK1 (Ser757) (#6888), ULK1 (D8H5) (#8054), Phospho-4EBP1 (Thr37/46) (#2855), 4E-BP1 (#9452), Phospho-mTOR (Ser2448) (#2971), rabbit anti-mTOR (7C10) (#2981), rabbit anti-LKB1 (27D10) (#3050), and Autophagy Atg8 Family Antibody Sampler Kit (#64459) were from Cell Signaling Technology; mouse anti-LBPA (C64) (MABT837) was from EMD Millipore; mouse anti-DNA antibody (#61014) was from Progen; mouse anti-LAMP2 (H4B4) and mouse anti-M6PR (22d4) were from Developmental Studies Hybridoma Bank (DSHB) at the University of Iowa.

Earle's Balanced Salt Solution (EBSS) (E3024) and hydrogen peroxide solution (H1009) were from Sigma-Aldrich. Bafilomycin A1 was from InvivoGen (Cat. Code: tlrl-baf1). CCCP (C2759), oligomycin A (#75351) and antimycin A (A8674) were from Sigma-Aldrich. LysoTracker™ Red DND-99 (L7528) and LysoTracker™ Green DND-26 (L7526) were from Thermo Fisher Scientific and used at 100 nM final concentration for 30 min.

Cell culture and transfection

HeLa, HEK293T, U2OS and THP-1 cells were from the American Type Culture Collection (ATCC). HeLa, HEK293T and U2OS cells were grown in Dulbecco's Modified Eagle's Medium (DMEM) supplemented with 10% fetal bovine serum (FBS), 2 mM L-glutamine, 10 mM HEPES, 1.0 mM sodium pyruvate, and 1 x penicillin–streptomycin (Thermo Fisher Scientific) at 37 °C in a 5% CO_2 atmosphere. THP-1 cells were grown in RPMI 1640 with 2 mM L-glutamine adjusted to contain 1.5 g/L sodium bicarbonate, 4.5 g/L glucose, 10 mM HEPES and 1.0 mM sodium pyruvate and supplemented with 0.05 mM β-mercaptoethanol (M6250, Sigma-Aldrich) and 10% FBS. The Huh7 cell line was from Rocky Mountain Laboratory. Keima reporter cell lines HEK293 RPS3-Keima

and HCT116 RPL28-Keima were from J. Wade Harper, Harvard University (An and Harper, 2018).

For Co-IP analysis of the interactions between over-expressed Stx16/Vti1a/Stx6 and mAtg8s, HEK293T cells in 10 cm petri dishes were transfected with corresponding plasmids via the ProFection Mammalian Transfection System (E1200, Promega). For other experiments, cells were transfected with Lipofectamine 2000 Transfection Reagent (# 11668-019, Thermo Fisher Scientific) according to the manufacturer's manual.

Plasmid constructs

STX16 plasmid was from DNASU (#HsCD00396980); STX6 was from Addgene (#31581); VTI1A DNA was PCR amplified from cDNA reverse transcribed from total RNAs isolated from HeLa cells. All constructs were transferred into pDEST-EGFP or pDEST-3XFLAG vectors using Gateway cloning system (#12535-019, Thermo Fisher Scientific), and verified by sequencing at GENEWIZ. EGFP-tagged LC3B and GABARAP constructed in pDEST vector were described before (Alemu et al., 2012). LIR-mutants of STX16 were generated with QuikChange Lightning Site-Directed Mutagenesis Kit (#210519, Agilent).

GST pull-down assay and peptide array analysis

Recombinant GST and GST-fusion proteins were expressed in competent *Escherichia coli* SoluBL21 (Genlantis, #C700200) by inducing overnight bacterial cultures with 50-75 μg/mL isopropyl β-D-1-thiogalactopyranoside (IPTG). Expressed proteins were purified by immobilization on Glutathione Sepharose 4 Fast Flow beads (GE Healthcare, #17-5132-01). For GST pull-down assays, myc-tagged proteins were *in vitro* translated in the presence of radioactive methionine (^{35}S-methionine) using the TNT T7 Reticulocyte Lysate System (Promega, #l4610). 10 μL of *in vitro* translated proteins were first precleared to remove unspecific binding with 10 μL of empty Glutathione Sepharose beads in 100 μL of NETN buffer (50 mM Tris pH 8.0, 150 mM NaCl, 1 mM EDTA, 0.5% NP-40) supplemented with cOmplete™ EDTA-free Protease Inhibitor Cocktail (Roche, #1183617001) for 30 min at 4 °C. This was followed by incubation of the precleared mixture with purified GST or GST-fusion proteins for 1-2 h at 4 °C. The mixture was washed five times with NETN buffer by centrifugation at 2500xg for 2 minutes followed by addition of 2XSDS gel-loading buffer (100 mM Tris pH 7.4, 4% SDS, 20% Glycerol, 0.2% Bromophenol blue and 200 mM dithiothreitol (DTT) (Sigma, #D0632) and heating for 10 minutes. The reaction was then resolved by SDS-PAGE and the gel stained with Coomassie Brilliant Blue R-250 Dye (Thermo Fisher Scientific, #20278) to visualize the GST and GST-fusion proteins. The gel was then vacuum-dried and radioactive signal detected by Bioimaging analyzer BAS-5000 (Fujifilm).

Peptide arrays of 20-mer amino acids of each SNARE protein were synthesized and immobilized on a membrane with the MultiPrep peptide synthesizer (Intavis Bioanalytical Instruments AG). The membrane was first blocked with 5% non-fat dry milk and then incubated with GST-GABARAP for 24 h. The membrane was washed three times and visualized by immunoblotting with anti-GST antibody as described (Rasmussen et al., 2019).

Generation of knockout cells with CRISPR/Cas9 gRNA

Sequences of gRNAs targeting *STX16* and *STX17* are shown in Fig. EV2A. *ATG3* gRNA target sequence: TAGTCCACCACTGTCCAACA; *STX6* gRNA target sequence: ACATGTCCCAGCGCATCGGA; *VTI1A* gRNA target sequence: AGATACCACCCCAAAGTCGA. All the single KO and *STX16/STX17* DKO HeLa, Huh7, U2OS, THP1 and HeLa-YFP-Parkin cells were generated by infecting target cells with single guide RNA (sgRNA) lentiviral vectors, lentiCRISPRv2, as described in (Sanjana et al., 2014). Briefly, HEK293T cells were transfected with lentiCRISPRv2 sgRNA vectors together with psPAX2 and pMD2.G at the ratio of 4 µg, 2.5 µg, 1.5 µg /6-cm dish. 60 hours later, the supernatants containing lentiviruses were collected and spun down at 1250 rpm for 5 min to clear cell debris. Lentiviruses were diluted with DMEM full medium at 1:2 ratio and used to infect target cells overnight with the presence of 8 µg/mL of polybrene (Hexadimethrine bromide, H9268, Sigma-Aldrich) in 12-well plates. Then the medium with lentivirus was removed and changed to fresh medium for another 24 hours. Cells were selected with puromycin (1 µg/mL) for 5 days before validation of the knockout. Single clones of HeLa, Huh7 and U2OS KO cells were isolated by seeding single cells in 96-well plates after serial dilutions. For THP1 KO cells, it is impossible to isolate single clones due to their suspension nature, and thus depletion of Stx16 and Stx17 was not complete. Data is shown in Fig EV3C. Generation of LC3 TKO, GABARAP TKO and Hexa KO HeLa cells was described as before (Nguyen et al., 2016b).

Western blotting and co-immunoprecipitation (Co-IP)

Cell lysates were prepared with a standard procedure using RIPA buffer (Pierce, #89900) supplemented with cOmplete™ EDTA-free Protease Inhibitor Cocktail (Roche, #1183617001). Protein concentrations were determined using Pierce™ BCA Protein Assay Kit (#23225). Protein electrophoresis was carried out using TGX™ SDS Gels (Bio-Rad, #4561091), followed by blotting to a nitrocellulose membrane (Bio-Rad, #1620112). Membranes were incubated with primary antibodies diluted in blocking buffer (3% BSA diluted in 1XTBS buffer plus 0.05% Tween-20) overnight at 4 °C. After incubation with fluorescently labeled secondary antibodies goat-anti-mouse IRDye 680LT or goat-anti-rabbit IRDye 800CW (LI-COR Biosciences) diluted 1: 10 000 in blocking buffer, membranes were scanned using a fluorescence scanner Odyssey (LI-COR Biosciences).

For Co-IP of overexpressed proteins, HEK293T cells cultured in 10-cm dishes were lysed with 1 mL NP-40 cell lysis buffer (Invitrogen, FNN0021). Cell lysates were spun down at top speed for 10 min at 4 °C to clear cell debris. The supernatants were collected and incubated with 2.5 µL anti-FLAG antibody (M2) for 4 hours, followed by incubation with Dynabeads® Protein G for 1 hour, and precipitated proteins were subjected to Western blot analysis with rabbit anti-GFP antibody. For endogenous Co-IP analysis, cell lysates were prepared from cells cultured in 15-cm dishes, and incubated with 2.5 µg mouse anti-Stx6 or mouse anti-LC3 antibody overnight at 4 °C, followed by Dynabeads® Protein G (Thermo Fisher Scientific, #10004D) binding and Western blot analysis of bound proteins.

Immunostaining and staining of acidified compartments for HCM and ImageStream flow cytometry

For HCM, cells were seeded in 96-well plates. After treatments, cells were washed once with 1X PBS, followed by fixation with 4% paraformaldehyde (PFA) for 5 min at room temperature. Cells were then permeabilized with 0.2% Triton X-100 for 10 min at room temperature. After incubation with blocking buffer (3% goat serum in 1X PBS), cells were stained with primary antibodies in blocking buffer for 1 h at room temperature or overnight at 4 °C, followed by staining with secondary antibodies (Alexa Fluro conjugates, Thermo Fisher Scientific) diluted 1:1000 in blocking buffer for 1 h at room temperature. For LysoTracker Red DND-99, cells in 96-well plates were cultured in full medium or starved for 1 h in EBSS, followed by adding LTR for another 30 min at the final concentration of 100 nM. For ImageStream flow cytometry analysis of LysoTracker Green DND-26, cells in 6-cm dishes were starved in EBSS for 1 h, followed by adding LTG for another 30 min at the final concentration of 100 nM. Cells were collected by trypsinization and resuspended in 200 µL 1X PBS for Amnis analysis.

High-content microscopy (HCM) computer-based image acquisition and quantification

High-content microscopy with automated image acquisition and quantification was carried out using a Cellomics ArrayScan VTI platform (Thermo Fisher Scientific). A minimum of 500 primary objects (valid cells) per well were imaged for the quantifications of intracellular targets (regions of interest, ROI). Scanning parameters and object masks were preset with HCS Studio Scan software for algorithm-defined automated image acquisition and analysis. The images were viewed, and ROI quantified with HCS View software iDEV provided with the Cellomics (Mandell et al., 2014).

ImageStream flow cytometry analysis

ImageStreamX Mark II flow cytometer Amnis® (EMD Millipore) was used to analyze LysoTracker Green DND-26 (LTG) staining after autophagy induction by

starvation. The 488 nm laser was used for excitation. Debris and doublets were gated out. Bright field (430–480 nm, Channel 01) and LTG (505–560 nm, Channel 02) channels were measured and at least 8,000 events of single cells per sample were collected. For analysis, the IDEAS version 6.0 software was used. Gating was applied to focused single cells using gradient root mean square of the bright field image then bright field area and aspect ratio, respectively. 50 cells with low/no fluorescent intensity and 50 cells with high fluorescent intensity and verified punctate LTG staining by image collection from WT cells were selected to create a template. The template was then applied to all other samples in the same experiment to generate quantifications (counts of LTG/cell) for each sample.

Electron microscopy

Wild type or *STX16/STX17*^{DKO} HeLa cells were grown in 6-cm dishes until they became semi-confluent. The cells were starved for 2 hours in EBSS, followed by fixation with 2% glutaraldehyde (EM grade) in 0.2 M HEPES, pH 7.4. After 30 min initial incubation, cells were scraped under a small volume of fixative and transferred to Eppendorf tubes. The tubes were spun at full speed for 10 min at room temperature to get a firm pellet. The pellets were continued being fixed until total fixation time is 2 h. Thin sections were cut using an ultramicrotome, collected onto electron microscopy grids and stained with uranyl acetate and lead citrate. In order to count autophagic compartments or Golgi apparatus, 47 images for each sample were taken at primary magnification of 5000X, using the principles of uniform random sampling. The images were zoomed on computer screen. Autophagic compartments and the Golgi apparatus were counted, and the cytoplasmic area was estimated by point counting (Eskelinen, 2008).

***M. tuberculosis* killing assay**

M. tuberculosis killing assay was carried out according to previously described (Kumar et al., 2018). Briefly, *Mycobacterium tuberculosis* Erdman (Erdman) culture was prepared by thawing frozen stock aliquot and grown in 7H9 Middlebrook liquid medium supplemented with oleic acid, albumin, dextrose and catalase (OADC, Becton Dickinson, Inc., Sparks, MD, USA), 0.5% glycerol and 0.05% Tween 80. Cultures were grown at 37°C. WT, *STX16*^{KO}, *STX17*^{KO}, and *STX16/STX17*^{DKO} THP1 cells (Fig. EV3C) were infected with Erdman at MOI 10 and incubated with full medium for 18 h or 16 h followed by starvation in EBSS for 2 h to induce autophagy, lysed, and plated on 7H11 agar plates. CFU was enumerated 3 weeks later.

Quantifications and Statistical analysis

Data, means ± SEM (n ≥ 3), were analyzed with paired and unpaired two-tailed Student's *t*-test, or by one-way or two-way ANOVA (analysis of variance)

followed by post hoc Tukey's test. Statistical significance was defined as: †, $p \geq 0.05$; *, $p < 0.05$; **, $p<0.01$.

Acknowledgements
We thank John Weaver and the AIM center, and J. Wade Harper for Keima cell lines, and Aurore Claude-Taupin for discussions. This work was supported by NIH grants R37AI042999, R01AI042999 and a center grant P20GM121176 to V.D. The work in the laboratory of T.J. was supported by Grant No. 190214 from the Norwegian Cancer Society and Grant No. 249884 from the Research Council of Norway to T.J.

Author contributions
Conceptualization, YG, TJ, SK, VD; Investigation and Validation, YG, VD, TJ; Methodology, YG, YPA, SK, BB, SWC, JJ, E-LE; Formal Analysis, YG, SK, VD, TJ; Resources, ML; Writing—Original Draft, YG, VD; Writing – Review and Editing, YG, VD, ML, TJ; Supervision, VD, TJ; Funding Acquisition, VD, TJ.

Conflict of interest
The authors declare that they have no conflict of interest.

REFERENCES

Alemu EA, Lamark T, Torgersen KM, Birgisdottir AB, Larsen KB, Jain A, Olsvik H, Overvatn A, Kirkin V, Johansen T (2012) ATG8 family proteins act as scaffolds for assembly of the ULK complex: sequence requirements for LC3-interacting region (LIR) motifs. *J Biol Chem* 287: 39275-90

An H, Harper JW (2018) Systematic analysis of ribophagy in human cells reveals bystander flux during selective autophagy. *Nature cell biology* 20: 135-143

Arasaki K, Nagashima H, Kurosawa Y, Kimura H, Nishida N, Dohmae N, Yamamoto A, Yanagi S, Wakana Y, Inoue H, Tagaya M (2018) MAP1B-LC1 prevents autophagosome formation by linking syntaxin 17 to microtubules. *EMBO Rep*

Arasaki K, Shimizu H, Mogari H, Nishida N, Hirota N, Furuno A, Kudo Y, Baba M, Baba N, Cheng J, Fujimoto T, Ishihara N, Ortiz-Sandoval C, Barlow LD, Raturi A, Dohmae N, Wakana Y, Inoue H, Tani K, Dacks JB et al. (2015) A role for the ancient SNARE syntaxin 17 in regulating mitochondrial division. *Dev Cell* 32: 304-17

Bakula D, Muller AJ, Zuleger T, Takacs Z, Franz-Wachtel M, Thost AK, Brigger D, Tschan MP, Frickey T, Robenek H, Macek B, Proikas-Cezanne T (2017) WIPI3 and WIPI4 beta-propellers are scaffolds for LKB1-AMPK-TSC signalling circuits in the control of autophagy. *Nat Commun* 8: 15637

Bas L, Papinski D, Licheva M, Torggler R, Rohringer S, Schuschnig M, Kraft C (2018) Reconstitution reveals Ykt6 as the autophagosomal SNARE in autophagosome-vacuole fusion. *J Cell Biol*

Baskaran S, Carlson LA, Stjepanovic G, Young LN, Kim do J, Grob P, Stanley RE, Nogales E, Hurley JH (2014) Architecture and dynamics of the autophagic phosphatidylinositol 3-kinase complex. *Elife* 3

Behrends C, Sowa ME, Gygi SP, Harper JW (2010) Network organization of the human autophagy system. *Nature* 466: 68-76

Betz C, Hall MN (2013) Where is mTOR and what is it doing there? *J Cell Biol* 203: 563-74

Bhujabal Z, Birgisdottir AB, Sjottem E, Brenne HB, Overvatn A, Habisov S, Kirkin V, Lamark T, Johansen T (2017) FKBP8 recruits LC3A to mediate Parkin-independent mitophagy. *EMBO Rep* 18: 947-961

Birgisdottir AB, Bhujabal Z, Wirth M, Sjøttem E, Evjen G, Zhang W, Lee R, O'Reilly N, Tooze SA, Lamark T, Johansen T (2019) Members of the autophagy class III phosphatidylinositol 3-kinase complex I
interact with GABARAP and GABARAPL1 via LIR motifs. *Autophagy* In press

Birgisdottir AB, Lamark T, Johansen T (2013) The LIR motif - crucial for selective autophagy. *Journal of cell science* 126: 3237-47

Bjorkoy G, Lamark T, Brech A, Outzen H, Perander M, Overvatn A, Stenmark H, Johansen T (2005) p62/SQSTM1 forms protein aggregates degraded by autophagy and has a protective effect on huntingtin-induced cell death. *J Cell Biol* 171: 603-14

Bright NA, Davis LJ, Luzio JP (2016) Endolysosomes Are the Principal Intracellular Sites of Acid Hydrolase Activity. *Curr Biol* 26: 2233-45
Carlsson SR, Simonsen A (2015) Membrane dynamics in autophagosome biogenesis. *Journal of cell science* 128: 193-205
Chang C, Young LN, Morris KL, von Bulow S, Schoneberg J, Yamamoto-Imoto H, Oe Y, Yamamoto K, Nakamura S, Stjepanovic G, Hummer G, Yoshimori T, Hurley JH (2019) Bidirectional Control of Autophagy by BECN1 BARA Domain Dynamics. *Mol Cell* 73: 339-353 e6
Cheng XT, Xie YX, Zhou B, Huang N, Farfel-Becker T, Sheng ZH (2018) Characterization of LAMP1-labeled nondegradative lysosomal and endocytic compartments in neurons. *J Cell Biol* 217: 3127-3139
Diao J, Liu R, Rong Y, Zhao M, Zhang J, Lai Y, Zhou Q, Wilz LM, Li J, Vivona S, Pfuetzner RA, Brunger AT, Zhong Q (2015) ATG14 promotes membrane tethering and fusion of autophagosomes to endolysosomes. *Nature* 520: 563-6
Dooley HC, Razi M, Polson HE, Girardin SE, Wilson MI, Tooze SA (2014) WIPI2 links LC3 conjugation with PI3P, autophagosome formation, and pathogen clearance by recruiting Atg12-5-16L1. *Mol Cell* 55: 238-52
Engedal N, Seglen PO (2016) Autophagy of cytoplasmic bulk cargo does not require LC3. *Autophagy* 12: 439-41
Eskelinen EL (2008) Fine structure of the autophagosome. *Methods Mol Biol* 445: 11-28
Florey O, Gammoh N, Kim SE, Jiang X, Overholtzer M (2015) V-ATPase and osmotic imbalances activate endolysosomal LC3 lipidation. *Autophagy* 11: 88-99
Fujita N, Morita E, Itoh T, Tanaka A, Nakaoka M, Osada Y, Umemoto T, Saitoh T, Nakatogawa H, Kobayashi S, Haraguchi T, Guan JL, Iwai K, Tokunaga F, Saito K, Ishibashi K, Akira S, Fukuda M, Noda T, Yoshimori T (2013) Recruitment of the autophagic machinery to endosomes during infection is mediated by ubiquitin. *J Cell Biol* 203: 115-28
Gammoh N, Florey O, Overholtzer M, Jiang X (2013) Interaction between FIP200 and ATG16L1 distinguishes ULK1 complex-dependent and -independent autophagy. *Nat Struct Mol Biol* 20: 144-9
Ganley IG, Espinosa E, Pfeffer SR (2008) A syntaxin 10-SNARE complex distinguishes two distinct transport routes from endosomes to the trans-Golgi in human cells. *J Cell Biol* 180: 159-72
Ganley IG, Lam du H, Wang J, Ding X, Chen S, Jiang X (2009) ULK1.ATG13.FIP200 complex mediates mTOR signaling and is essential for autophagy. *J Biol Chem* 284: 12297-305
Gao J, Reggiori F, Ungermann C (2018) A novel in vitro assay reveals SNARE topology and the role of Ykt6 in autophagosome fusion with vacuoles. *J Cell Biol*
Garcia D, Shaw RJ (2017) AMPK: Mechanisms of Cellular Energy Sensing and Restoration of Metabolic Balance. *Mol Cell* 66: 789-800
Gatica D, Lahiri V, Klionsky DJ (2018) Cargo recognition and degradation by selective autophagy. *Nature cell biology* 20: 233-242
Gingras AC, Gygi SP, Raught B, Polakiewicz RD, Abraham RT, Hoekstra MF, Aebersold R, Sonenberg N (1999) Regulation of 4E-BP1 phosphorylation: a novel two-step mechanism. *Genes Dev* 13: 1422-37

Guo B, Liang Q, Li L, Hu Z, Wu F, Zhang P, Ma Y, Zhao B, Kovacs AL, Zhang Z, Feng D, Chen S, Zhang H (2014) O-GlcNAc-modification of SNAP-29 regulates autophagosome maturation. *Nature cell biology* 16: 1215-26
Guo H, Chitiprolu M, Roncevic L, Javalet C, Hemming FJ, Trung MT, Meng L, Latreille E, Tanese de Souza C, McCulloch D, Baldwin RM, Auer R, Cote J, Russell RC, Sadoul R, Gibbings D (2017) Atg5 Disassociates the V1V0-ATPase to Promote Exosome Production and Tumor Metastasis Independent of Canonical Macroautophagy. *Dev Cell* 43: 716-730 e7
Gutierrez MG, Master SS, Singh SB, Taylor GA, Colombo MI, Deretic V (2004) Autophagy is a defense mechanism inhibiting BCG and Mycobacterium tuberculosis survival in infected macrophages. *Cell* 119: 753-66
Hamasaki M, Furuta N, Matsuda A, Nezu A, Yamamoto A, Fujita N, Oomori H, Noda T, Haraguchi T, Hiraoka Y, Amano A, Yoshimori T (2013) Autophagosomes form at ER-mitochondria contact sites. *Nature* 495: 389-93
Hatsuzawa K, Hirose H, Tani K, Yamamoto A, Scheller RH, Tagaya M (2000) Syntaxin 18, a SNAP Receptor That Functions in the Endoplasmic Reticulum, Intermediate Compartment, and cis-Golgi Vesicle Trafficking. *Journal of Biological Chemistry* 275: 13713-13720
He C, Levine B (2010) The Beclin 1 interactome. *Current opinion in cell biology* 22: 140-9
Hong W, Lev S (2014) Tethering the assembly of SNARE complexes. *Trends in cell biology* 24: 35-43
Hosokawa N, Hara T, Kaizuka T, Kishi C, Takamura A, Miura Y, Iemura S, Natsume T, Takehana K, Yamada N, Guan JL, Oshiro N, Mizushima N (2009) Nutrient-dependent mTORC1 association with the ULK1-Atg13-FIP200 complex required for autophagy. *Molecular biology of the cell* 20: 1981-91
Itakura E, Kishi-Itakura C, Mizushima N (2012) The hairpin-type tail-anchored SNARE syntaxin 17 targets to autophagosomes for fusion with endosomes/lysosomes. *Cell* 151: 1256-69
Jahn R, Scheller RH (2006) SNAREs--engines for membrane fusion. *Nature reviews Molecular cell biology* 7: 631-43
Jao CC, Ragusa MJ, Stanley RE, Hurley JH (2013) A HORMA domain in Atg13 mediates PI 3-kinase recruitment in autophagy. *Proc Natl Acad Sci U S A* 110: 5486-91
Jung CH, Jun CB, Ro SH, Kim YM, Otto NM, Cao J, Kundu M, Kim DH (2009) ULK-Atg13-FIP200 complexes mediate mTOR signaling to the autophagy machinery. *Molecular biology of the cell* 20: 1992-2003
Kabeya Y, Mizushima N, Ueno T, Yamamoto A, Kirisako T, Noda T, Kominami E, Ohsumi Y, Yoshimori T (2000) LC3, a mammalian homologue of yeast Apg8p, is localized in autophagosome membranes after processing. *Embo J* 19: 5720-8
Katayama H, Kogure T, Mizushima N, Yoshimori T, Miyawaki A (2011) A sensitive and quantitative technique for detecting autophagic events based on lysosomal delivery. *Chemistry & biology* 18: 1042-52
Keown JR, Black MM, Ferron A, Yap M, Barnett MJ, Pearce FG, Stoye JP, Goldstone DC (2018) A helical LC3-interacting region mediates the interaction

between the retroviral restriction factor Trim5alpha and mammalian autophagy-related ATG8 proteins. *J Biol Chem* 293: 18378-18386
Kim J, Kim YC, Fang C, Russell RC, Kim JH, Fan W, Liu R, Zhong Q, Guan KL (2013) Differential regulation of distinct Vps34 complexes by AMPK in nutrient stress and autophagy. *Cell* 152: 290-303
Kim J, Kundu M, Viollet B, Guan KL (2011) AMPK and mTOR regulate autophagy through direct phosphorylation of Ulk1. *Nature cell biology* 13: 132-41
Kimura T, Jia J, Kumar S, Choi SW, Gu Y, Mudd M, Dupont N, Jiang S, Peters R, Farzam F, Jain A, Lidke KA, Adams CM, Johansen T, Deretic V (2017) Dedicated SNAREs and specialized TRIM cargo receptors mediate secretory autophagy. *EMBO J* 36: 42-60
Kimura T, Mandell M, Deretic V (2016) Precision autophagy directed by receptor regulators - emerging examples within the TRIM family. *Journal of cell science* 129: 881-91
Kirisako T, Baba M, Ishihara N, Miyazawa K, Ohsumi M, Yoshimori T, Noda T, Ohsumi Y (1999) Formation process of autophagosome is traced with Apg8/Aut7p in yeast. *J Cell Biol* 147: 435-46
Klionsky DJ, Abdelmohsen K, Abe A, Abedin MJ, Abeliovich H, Acevedo Arozena A, Adachi H, Adams CM, Adams PD, Adeli K, Adhihetty PJ, Adler SG, Agam G, Agarwal R, Aghi MK, Agnello M, Agostinis P, Aguilar PV, Aguirre-Ghiso J, Airoldi EM et al. (2016) Guidelines for the use and interpretation of assays for monitoring autophagy (3rd edition). *Autophagy* 12: 1-222
Klionsky DJ, Abeliovich H, Agostinis P, Agrawal DK, Aliev G, Askew DS, Baba M, Baehrecke EH, Bahr BA, Ballabio A, Bamber BA, Bassham DC, Bergamini E, Bi X, Biard-Piechaczyk M, Blum JS, Bredesen DE, Brodsky JL, Brumell JH, Brunk UT et al. (2008) Guidelines for the use and interpretation of assays for monitoring autophagy in higher eukaryotes. *Autophagy* 4: 151-75
Kriegenburg F, Ungermann C, Reggiori F (2018) Coordination of Autophagosome-Lysosome Fusion by Atg8 Family Members. *Curr Biol* 28: R512-R518
Kumar S, al. e (2019) Phosphorylation of Syntaxin 17 by TBK1 controls autophagy initiation *Developmental Cell* In press
Kumar S, Jain A, Farzam F, Jia J, Gu Y, Choi SW, Mudd MH, Claude-Taupin A, Wester MJ, Lidke KA, Rusten TE, Deretic V (2018) Mechanism of Stx17 recruitment to autophagosomes via IRGM and mammalian Atg8 proteins. *J Cell Biol* 217: 997-1013
Lawrence RE, Zoncu R (2019) The lysosome as a cellular centre for signalling, metabolism and quality control. *Nature cell biology*
Lazarou M, Sliter DA, Kane LA, Sarraf SA, Wang C, Burman JL, Sideris DP, Fogel AI, Youle RJ (2015) The ubiquitin kinase PINK1 recruits autophagy receptors to induce mitophagy. *Nature* 524: 309-14
Levine B, Kroemer G (2019) Biological Functions of Autophagy Genes: A Disease Perspective. *Cell* 176: 11-42
Lippincott-Schwartz J, Fambrough DM (1987) Cycling of the integral membrane glycoprotein, LEP100, between plasma membrane and lysosomes: kinetic and morphological analysis. *Cell* 49: 669-77

Liu L, Feng D, Chen G, Chen M, Zheng Q, Song P, Ma Q, Zhu C, Wang R, Qi W, Huang L, Xue P, Li B, Wang X, Jin H, Wang J, Yang F, Liu P, Zhu Y, Sui S et al. (2012) Mitochondrial outer-membrane protein FUNDC1 mediates hypoxia-induced mitophagy in mammalian cells. *Nature cell biology* 14: 177-85
Low SH, Chapin SJ, Weimbs T, Komuves LG, Bennett MK, Mostov KE (1996) Differential localization of syntaxin isoforms in polarized Madin-Darby canine kidney cells. *Molecular biology of the cell* 7: 2007-18
Luzio JP, Rous BA, Bright NA, Pryor PR, Mullock BM, Piper RC (2000) Lysosome-endosome fusion and lysosome biogenesis. *Journal of cell science* 113: 1515-24
Mallard F, Tang BL, Galli T, Tenza D, Saint-Pol A, Yue X, Antony C, Hong W, Goud B, Johannes L (2002) Early/recycling endosomes-to-TGN transport involves two SNARE complexes and a Rab6 isoform. *J Cell Biol* 156: 653-64
Malsam J, Söllner TH (2011) Organization of SNAREs within the Golgi Stack. *Cold Spring Harbor Perspectives in Biology*
Mandell MA, Jain A, Arko-Mensah J, Chauhan S, Kimura T, Dinkins C, Silvestri G, Munch J, Kirchhoff F, Simonsen A, Wei Y, Levine B, Johansen T, Deretic V (2014) TRIM proteins regulate autophagy and can target autophagic substrates by direct recognition. *Dev Cell* 30: 394-409
Manjithaya R, Nazarko TY, Farre JC, Subramani S (2010) Molecular mechanism and physiological role of pexophagy. *FEBS letters* 584: 1367-73
Marino G, Pietrocola F, Eisenberg T, Kong Y, Malik SA, Andryushkova A, Schroeder S, Pendl T, Harger A, Niso-Santano M, Zamzami N, Scoazec M, Durand S, Enot DP, Fernandez AF, Martins I, Kepp O, Senovilla L, Bauvy C, Morselli E et al. (2014) Regulation of autophagy by cytosolic acetyl-coenzyme A. *Mol Cell* 53: 710-25
Matsui T, Jiang P, Nakano S, Sakamaki Y, Yamamoto H, Mizushima N (2018) Autophagosomal YKT6 is required for fusion with lysosomes independently of syntaxin 17. *J Cell Biol* 217: 2633-2645
McEwan DG, Popovic D, Gubas A, Terawaki S, Suzuki H, Stadel D, Coxon FP, Miranda de Stegmann D, Bhogaraju S, Maddi K, Kirchof A, Gatti E, Helfrich MH, Wakatsuki S, Behrends C, Pierre P, Dikic I (2015) PLEKHM1 regulates autophagosome-lysosome fusion through HOPS complex and LC3/GABARAP proteins. *Mol Cell* 57: 39-54
Mizushima N, Noda T, Yoshimori T, Tanaka Y, Ishii T, George MD, Klionsky DJ, Ohsumi M, Ohsumi Y (1998a) A protein conjugation system essential for autophagy. *Nature* 395: 395-8
Mizushima N, Sugita H, Yoshimori T, Ohsumi Y (1998b) A new protein conjugation system in human. The counterpart of the yeast Apg12p conjugation system essential for autophagy. *J Biol Chem* 273: 33889-92
Mizushima N, Yoshimori T, Ohsumi Y (2011) The role of Atg proteins in autophagosome formation. *Annu Rev Cell Dev Biol* 27: 107-32
Moreau K, Renna M, Rubinsztein DC (2013) Connections between SNAREs and autophagy. *Trends Biochem Sci* 38: 57-63
Muller JM, Shorter J, Newman R, Deinhardt K, Sagiv Y, Elazar Z, Warren G, Shima DT (2002) Sequential SNARE disassembly and GATE-16-GOS-28

complex assembly mediated by distinct NSF activities drives Golgi membrane fusion. *J Cell Biol* 157: 1161-73
Nair U, Jotwani A, Geng J, Gammoh N, Richerson D, Yen WL, Griffith J, Nag S, Wang K, Moss T, Baba M, McNew JA, Jiang X, Reggiori F, Melia TJ, Klionsky DJ (2011) SNARE proteins are required for macroautophagy. *Cell* 146: 290-302
Nakamura S, Yoshimori T (2017) New insights into autophagosome-lysosome fusion. *Journal of cell science* 130: 1209-1216
Nakatogawa H, Ichimura Y, Ohsumi Y (2007) Atg8, a ubiquitin-like protein required for autophagosome formation, mediates membrane tethering and hemifusion. *Cell* 130: 165-78
Nguyen TN, Padman BS, Lazarou M (2016a) Deciphering the Molecular Signals of PINK1/Parkin Mitophagy. *Trends in cell biology* 26: 733-744
Nguyen TN, Padman BS, Usher J, Oorschot V, Ramm G, Lazarou M (2016b) Atg8 family LC3/GABARAP proteins are crucial for autophagosome-lysosome fusion but not autophagosome formation during PINK1/Parkin mitophagy and starvation. *J Cell Biol* 215: 857-874
Nishimura T, Kaizuka T, Cadwell K, Sahani MH, Saitoh T, Akira S, Virgin HW, Mizushima N (2013) FIP200 regulates targeting of Atg16L1 to the isolation membrane. *EMBO Rep* 14: 284-91
Noda T, Ohsumi Y (1998) Tor, a phosphatidylinositol kinase homologue, controls autophagy in yeast. *J Biol Chem* 273: 3963-6
Olsvik HL, Lamark T, Takagi K, Bowitz Larsen K, Evjen G, Overvatn A, Mizushima T, Johansen T (2015) FYCO1 Contains a C-terminally Extended, LC3A/B-preferring LC3-Interacting Region (LIR) Motif Required for Efficient Maturation of Autophagosomes During Basal Autophagy. *J Biol Chem*
Park JM, Jung CH, Seo M, Otto NM, Grunwald D, Kim KH, Moriarity B, Kim YM, Starker C, Nho RS, Voytas D, Kim DH (2016) The ULK1 complex mediates MTORC1 signaling to the autophagy initiation machinery via binding and phosphorylating ATG14. *Autophagy* 12: 547-64
Petiot A, Ogier-Denis E, Blommaart EF, Meijer AJ, Codogno P (2000) Distinct classes of phosphatidylinositol 3'-kinases are involved in signaling pathways that control macroautophagy in HT-29 cells. *J Biol Chem* 275: 992-8.
Pols MS, van Meel E, Oorschot V, ten Brink C, Fukuda M, Swetha MG, Mayor S, Klumperman J (2013) hVps41 and VAMP7 function in direct TGN to late endosome transport of lysosomal membrane proteins. *Nat Commun* 4: 1361
Ponpuak M, Mandell MA, Kimura T, Chauhan S, Cleyrat C, Deretic V (2015) Secretory autophagy. *Curr Opin Cell Biol* 35: 106-116
Popelka H, Klionsky DJ (2015) Analysis of the native conformation of the LIR/AIM motif in the Atg8/LC3/GABARAP-binding proteins. *Autophagy* 11: 2153-9
Randow F, Youle RJ (2014) Self and nonself: how autophagy targets mitochondria and bacteria. *Cell Host Microbe* 15: 403-11
Rasmussen MS, Birgisdottir AB, Johansen T (2019) Use of Peptide Arrays for Identification and Characterization of LIR Motifs. *Methods Mol Biol* 1880: 149-161

Rogov V, Dotsch V, Johansen T, Kirkin V (2014) Interactions between autophagy receptors and ubiquitin-like proteins form the molecular basis for selective autophagy. *Mol Cell* 53: 167-78
Rogov VV, Stolz A, Ravichandran AC, Rios-Szwed DO, Suzuki H, Kniss A, Lohr F, Wakatsuki S, Dotsch V, Dikic I, Dobson RC, McEwan DG (2017) Structural and functional analysis of the GABARAP interaction motif (GIM). *EMBO Rep* 18: 1382-1396
Saftig P, Klumperman J (2009) Lysosome biogenesis and lysosomal membrane proteins: trafficking meets function. *Nature reviews Molecular cell biology* 10: 623-35
Sagiv Y, Legesse-Miller A, Porat A, Elazar Z (2000) GATE-16, a membrane transport modulator, interacts with NSF and the Golgi v-SNARE GOS-28. *EMBO J* 19: 1494-504
Sancak Y, Bar-Peled L, Zoncu R, Markhard AL, Nada S, Sabatini DM (2010) Ragulator-Rag complex targets mTORC1 to the lysosomal surface and is necessary for its activation by amino acids. *Cell* 141: 290-303
Sandoval H, Thiagarajan P, Dasgupta SK, Schumacher A, Prchal JT, Chen M, Wang J (2008) Essential role for Nix in autophagic maturation of erythroid cells. *Nature* 454: 232-5
Sanjana NE, Shalem O, Zhang F (2014) Improved vectors and genome-wide libraries for CRISPR screening. *Nat Methods* 11: 783-784
Sanjuan MA, Dillon CP, Tait SW, Moshiach S, Dorsey F, Connell S, Komatsu M, Tanaka K, Cleveland JL, Withoff S, Green DR (2007) Toll-like receptor signalling in macrophages links the autophagy pathway to phagocytosis. *Nature* 450: 1253-7
Saxton RA, Sabatini DM (2017) mTOR Signaling in Growth, Metabolism, and Disease. *Cell* 168: 960-976
Scott RC, Schuldiner O, Neufeld TP (2004) Role and regulation of starvation-induced autophagy in the Drosophila fat body. *Dev Cell* 7: 167-78
Seglen PO, Luhr M, Mills IG, Saetre F, Szalai P, Engedal N (2015) Macroautophagic cargo sequestration assays. *Methods* 75: 25-36
Shpilka T, Weidberg H, Pietrokovski S, Elazar Z (2011) Atg8: an autophagy-related ubiquitin-like protein family. *Genome Biol* 12: 226
Skytte Rasmussen M, Mouilleron S, Kumar Shrestha B, Wirth M, Lee R, Bowitz Larsen K, Abudu Princely Y, O'Reilly N, Sjottem E, Tooze SA, Lamark T, Johansen T (2017) ATG4B contains a C-terminal LIR motif important for binding and efficient cleavage of mammalian orthologs of yeast Atg8. *Autophagy* 13: 834-853
Stadel D, Millarte V, Tillmann KD, Huber J, Tamin-Yecheskel BC, Akutsu M, Demishtein A, Ben-Zeev B, Anikster Y, Perez F, Dotsch V, Elazar Z, Rogov V, Farhan H, Behrends C (2015) TECPR2 Cooperates with LC3C to Regulate COPII-Dependent ER Export. *Mol Cell* 60: 89-104
Stolz A, Ernst A, Dikic I (2014) Cargo recognition and trafficking in selective autophagy. *Nature cell biology* 16: 495-501

Subramaniam VN, Peter F, Philp R, Wong SH, Hong W (1996) GS28, a 28-Kilodalton Golgi SNARE That Participates in ER-Golgi Transport. *Science* 272: 1161-1163
Tai G, Lu L, Wang TL, Tang BL, Goud B, Johannes L, Hong W (2004) Participation of the syntaxin 5/Ykt6/GS28/GS15 SNARE complex in transport from the early/recycling endosome to the trans-Golgi network. *Molecular biology of the cell* 15: 4011-22
Takats S, Glatz G, Szenci G, Boda A, Horvath GV, Hegedus K, Kovacs AL, Juhasz G (2018) Non-canonical role of the SNARE protein Ykt6 in autophagosome-lysosome fusion. *PLoS Genet* 14: e1007359
Takats S, Nagy P, Varga A, Pircs K, Karpati M, Varga K, Kovacs AL, Hegedus K, Juhasz G (2013) Autophagosomal Syntaxin17-dependent lysosomal degradation maintains neuronal function in Drosophila. *J Cell Biol* 201: 531-9
Tan X, Liao Z, Liang H, Chen X, Zhang B, Chu L (2018) Upregulation of liver kinase B1 predicts poor prognosis in hepatocellular carcinoma. *International journal of oncology* 53: 1913-1926
Tanaka Y, Guhde G, Suter A, Eskelinen EL, Hartmann D, Lullmann-Rauch R, Janssen PM, Blanz J, von Figura K, Saftig P (2000) Accumulation of autophagic vacuoles and cardiomyopathy in LAMP-2-deficient mice. *Nature* 406: 902-6
Tsuboyama K, Koyama-Honda I, Sakamaki Y, Koike M, Morishita H, Mizushima N (2016) The ATG conjugation systems are important for degradation of the inner autophagosomal membrane. *Science* 354: 1036-1041
Velikkakath AK, Nishimura T, Oita E, Ishihara N, Mizushima N (2012) Mammalian Atg2 proteins are essential for autophagosome formation and important for regulation of size and distribution of lipid droplets. *Molecular biology of the cell* 23: 896-909
Violot S, Carpentier P, Blanchoin L, Bourgeois D (2009) Reverse pH-dependence of chromophore protonation explains the large Stokes shift of the red fluorescent protein mKeima. *J Am Chem Soc* 131: 10356-7
von Muhlinen N, Akutsu M, Ravenhill BJ, Foeglein A, Bloor S, Rutherford TJ, Freund SM, Komander D, Randow F (2012) LC3C, Bound Selectively by a Noncanonical LIR Motif in NDP52, Is Required for Antibacterial Autophagy. *Molecular cell* 48: 329-42
Wang Y, Foo LY, Guo K, Gan BQ, Zeng Q, Hong W, Tang BL (2006) Syntaxin 9 is Enriched in Skin Hair Follicle Epithelium and Interacts With the Epidermal Growth Factor Receptor. *Traffic* 7: 216-226
Wang Z, Miao G, Xue X, Guo X, Yuan C, Wang Z, Zhang G, Chen Y, Feng D, Hu J, Zhang H (2016) The Vici Syndrome Protein EPG5 Is a Rab7 Effector that Determines the Fusion Specificity of Autophagosomes with Late Endosomes/Lysosomes. *Mol Cell* 63: 781-95
Wei Y, Chiang WC, Sumpter R, Jr., Mishra P, Levine B (2017) Prohibitin 2 Is an Inner Mitochondrial Membrane Mitophagy Receptor. *Cell* 168: 224-238 e10
Weidberg H, Shpilka T, Shvets E, Abada A, Shimron F, Elazar Z (2011) LC3 and GATE-16 N termini mediate membrane fusion processes required for autophagosome biogenesis. *Developmental cell* 20: 444-54

Weidberg H, Shvets E, Shpilka T, Shimron F, Shinder V, Elazar Z (2010) LC3 and GATE-16/GABARAP subfamilies are both essential yet act differently in autophagosome biogenesis. *The EMBO journal* 29: 1792-802

Wild P, Farhan H, McEwan DG, Wagner S, Rogov VV, Brady NR, Richter B, Korac J, Waidmann O, Choudhary C, Dotsch V, Bumann D, Dikic I (2011) Phosphorylation of the autophagy receptor optineurin restricts Salmonella growth. *Science* 333: 228-33

Wubbolts R, Fernandez-Borja M, Oomen L, Verwoerd D, Janssen H, Calafat J, Tulp A, Dusseljee S, Neefjes J (1996) Direct vesicular transport of MHC class II molecules from lysosomal structures to the cell surface. *J Cell Biol* 135: 611-22

Xie Z, Nair U, Klionsky DJ (2008) Atg8 controls phagophore expansion during autophagosome formation. *Molecular biology of the cell* 19: 3290-8

Youle RJ, Narendra DP (2011) Mechanisms of mitophagy. *Nature reviews Molecular cell biology* 12: 9-14

Young AR, Chan EY, Hu XW, Kochl R, Crawshaw SG, High S, Hailey DW, Lippincott-Schwartz J, Tooze SA (2006) Starvation and ULK1-dependent cycling of mammalian Atg9 between the TGN and endosomes. *Journal of cell science* 119: 3888-900

Zhang J, Tripathi DN, Jing J, Alexander A, Kim J, Powell RT, Dere R, Tait-Mulder J, Lee JH, Paull TT, Pandita RK, Charaka VK, Pandita TK, Kastan MB, Walker CL (2015) ATM functions at the peroxisome to induce pexophagy in response to ROS. *Nature cell biology* 17: 1259-1269

Figure 1. Many SNAREs bind mammalian Atg8 proteins

(A) Peptide array dot blot analysis to identify LIR motifs in the indicated SNARE proteins. Amino acids for the identified LIRs from positive signals are marked on each SNARE. Amino acids are denoted as amino acid single letter codes in the blot.

(B) Schematics of the functional domains of Stx16/Vti1a/Stx6 cognate SNAREs with the positions of LIR motifs. The LIR motif marked in green in syntaxin 16 indicates established LIR based on following analyses.

(C) Co-immunoprecipitation (Co-IP) analysis of interactions between FLAG-tagged Stx16/Vti1a/Stx6 and EGFP-tagged LC3B or GABARAP overexpressed in HEK293T cells. * indicates mouse IgG heavy chain of precipitated mouse-anti-FLAG antibody.

(D) GST pull-down analysis of interactions between radiolabeled Myc-Stx16 and GST-tagged mAtg8 proteins.

(E) GST pull-down analysis of interactions between wild type (WT) or LIR-mutant (L219A/V222A) Stx16 and GST-tagged LC3C or GABARAP. Lower panel shows percentages of WT or LIR-mutant Stx16 bound to GST-LC3C or GST-GABARAP. Data shown as means ± SEM of precipitated Stx16, n = 3.

(F) GST pull-down analysis of interactions between WT or different types of LIR-mutant Stx16 and GST-tagged LC3C or GABARAP. Lower panel shows percentages of WT or LIR-mutant Stx16 bound to GST-LC3C or GST-GABARAP.

(G) GST pull-down analysis of interactions between radiolabeled Myc-Stx16 and WT or LDS-mutant GABARAP (GABARAP-Y49A and -Y49A/F104A). Lower panel shows percentages of Stx16 bound to WT or LDS-mutant GABARAP. Data shown as means ± SEM of precipitated Stx16, n = 3.

Figure 2. The mAtg8-interacting SNAREs Stx16 and Stx17 are required for efficient bulk autophagic flux

(A) WT or *STX17*-knockout (*STX17*^{KO}) HeLa cells were starved with or without the presence of bafilomycin A1 (Baf A1, 100 nM) for 2 h, and cell lysates were subjected to Western blot analysis of LC3B and p62.

(B) Quantifications of LC3B-II levels normalized to β-actin from cells treated as in (A); Data shown as means ± SEM of LC3B-II and β-actin ratios, n = 3; *, $p < 0.05$ (one-way ANOVA).

(C) WT, *STX16*^{KO}, *STX17*^{KO} or *STX16/STX17* double KO (*STX16/STX17*^{DKO}) HeLa cells were starved with or without the presence of Baf A1 (100 nM) for 2 h, and cell lysates were subjected to Western blot analysis of LC3B.

(D) Quantifications of LC3B-II levels normalized to β-actin from (C); Data shown as means ± SEM of LC3B-II and β-actin ratios, n = 3; †, not significant; **, $p < 0.01$ (one-way ANOVA).

(E) WT or *STX16/STX17*^{DKO} HeLa cells were starved in EBSS for 2 h, and subjected to ultrastructural analysis of the autophagic vesicles (AV) with electron microscopy. AVi: initial autophagic vacuoles; AVd: degradative autophagic vacuoles; G: Golgi apparatus. Image acquisition and counting as in Methods. Scale bars, 1 μm and 0.5 μm (top sections).

(F) Quantifications of autophagic vesicles in WT and *STX16/STX17*^{DKO} HeLa cells treated as (E); Data shown as means ± SEM of AV profiles relative to cytoplasmic area; †, not significant; *, $p < 0.05$ (two-way ANOVA). AV profiles from 47 images of each samples were counted.

Figure 3. Stx16 and Stx17 are required for selective autophagy of mitochondria, peroxisomes, and *M. tuberculosis*

(A) WT or *STX16/STX17*^{DKO} HeLa-YFP-Parkin cells were treated with CCCP (10 μM) or oligomycin A (5 μM) and antimycin A (10 μM) (OA) for 16 hours, and subjected to high-content microscopy (HCM) analysis of mitochondria clearance. Masks: blue, nuclei; red, mitochondria stained with mitochondrial DNA (mtDNA) antibody. Scale bar: 20 μm.

(B) Quantifications of mtDNA by object count or total area per cell in WT or *STX16/STX17*^{DKO} HeLa-YFP-Parkin cells treated as in (A); Data shown as means ± SEM of mtDNA object count (upper panel) or object total area (lower panel) per cell; minimum 500 cells were counted each well from at least 12 wells, 3 independent experiments; **, $p < 0.01$ (two-way ANOVA).

(C) WT or *STX16/STX17*^{DKO} Huh7 cells were treated with H_2O_2 (0.4 mM) for indicated time points, and autophagic clearance of peroxisomes was measured by the protein levels of PMP70, PEX14 and p62.

(D) Quantifications of peroxisomal proteins PMP70 and PEX14 for WT or *STX16/STX17*^{DKO} Huh7 cells treated as in (C); Data shown as means ± SEM of PEX14 or PMP70 and β-actin ratios, n = 3; †, not significant; *, $p < 0.05$; **, $p < 0.01$ (two-way ANOVA).

(E) WT, *STX16*^{KO}, *STX17*^{KO} or *STX16/STX17*^{DKO} THP-1 cells were infected with *Mycobacterium tuberculosis* (*Mtb*), followed by starvation to induce autophagy. Autophagic clearance of infected *Mtb* was measured by *Mtb* colonies grown on Middlebrook 7H11 agar plates; Data shown as means ± SEM of *Mtb* colonies, n = 4; *, $p < 0.05$; **, $p < 0.01$ (two-way ANOVA).

(F) Schematics for the requirement of Stx16 and Stx17 in autophagic clearance of damaged mitochondria, surplus peroxisomes and invaded bacterial pathogens.

Figure 4. Stx16 and Stx17 cooperate in ribophagy

(A) Schematic of ribophagy detection with Keima-based reporter system; FP: fluorescent protein.

(B) Validation of *STX16/STX17* DKO by Western blot analysis in HEK293 cells stably expressing RPS3-Keima (left panel) and HCT116 cells stably expressing RPL28-Keima (right panel).

(C) WT or *STX16/STX17*^{DKO} HEK293 RPS3-Keima cells were cultured in full medium or starved for 8 hours, and subjected to HCM analysis of Keima puncta accumulated in autolysosomes with the excitation wavelength at 560 nm. Masks: white, cells identified based on nuclei; red, Keima puncta detected with the excitation and emission wavelengths of 560 nm and 620 nm, respectively; lower panel shows Keima puncta without masks. Scale bar: 20 μm.

(D) Quantifications of autolysosomal Keima puncta in WT or *STX16/STX17*^{DKO} HEK293 RPS3-Keima cells treated as in (C). Data shown as means ± SEM of Keima puncta per cell, minimum 1000 cells were counted each well from at least 12 wells, 3 independent experiments; **, $p < 0.01$ (two-way ANOVA).

(E) WT or *STX16/STX17*^{DKO} HCT116 RPL28-Keima cells were cultured in full medium or starved for 8 hours, and subjected to HCM analysis of Keima puncta accumulated in autolysosomes with the excitation wavelength at 560 nm. Masks: white, cells identified based on nuclei; red, Keima puncta detected with the excitation and emission wavelengths of 560 nm and 620 nm, respectively; lower panel shows Keima puncta without masks. Scale bar: 20 μm.

(F) Quantifications of autolysosomal Keima puncta in WT or *STX16/STX17*^{DKO} HCT116 RPL28-Keima cells treated as in (E). Data shown as means ± SEM of Keima puncta per cell, minimum 1000 cells were counted each well from at least 12 wells, 3 independent experiments; †, not significant; **, $p < 0.01$ (two-way ANOVA).

Figure 5. Stx16 is required for the maintenance of lysosomal homeostasis and mTOR activity

(A) WT or *STX16*^{KO} HeLa cells were starved in EBSS for 2 h and subjected to HCM analysis of LAMP2 and LC3 puncta. Masks: white, cells identified based on nuclei; red, LC3 puncta; green, LAMP2 puncta; yellow, overlap of LC3 and LAMP2. Scale bar: 20 μm.

(B–D) Quantifications of LC3 puncta per cell (B), LC3 and LAMP2 overlap area per cell (C), and LAMP2 puncta per cell (D) in WT or *STX16*^{KO} cells treated as in (A). Data shown as means ± SEM of puncta or overlap area per cell, minimum 500 cells were counted each well from at least 12 wells, 3 independent experiments; *, $p < 0.05$; **, $p < 0.01$ (two-way ANOVA).

(E) Western blot analysis of LAMP1 and LAMP2 protein levels in WT and separate clones of *STX16*^{KO} HeLa, Huh7, and U2OS cells.

(F) Western blot analysis of LAMP2 protein levels in WT and separate clones of *STX6*^{KO} or *VTI1A*^{KO} HeLa cells.

(G) Time course of mTOR inactivation during EBSS starvation in WT vs. *STX16*^{KO} HeLa cells analyzed by Western blotting for mTOR substrates ULK1 and 4E-BP1.

(H) WT or *STX16*^{KO} HeLa cells were starved in EBSS for 1 h and subjected to HCM analysis of mTOR puncta. Masks: white, cells identified based on nuclei; red, mTOR puncta. Scale bar: 20 μm.

(I) Quantifications of mTOR puncta in WT or *STX16*^{KO} cells treated as in (H). Data shown as means ± SEM of mTOR puncta per cell, minimum 500 cells were counted each well from at least 12 wells, 3 independent experiments; **, $p < 0.01$ (two-way ANOVA).

Figure 6. Stx16 regulates proper distribution of acidified compartments in the cell

(A) WT or *STX16*^{KO} HeLa cells were starved in EBSS for 1 h, followed by starvation with the presence of LysoTracker Red DND-99 (LTR) (100 nM) for additional 30 min, and subjected to HCM analysis of LTR. Scale bar: 20 μm.

(B) Quantifications of LTR count per cell or total area per cell in WT and *STX16*^{KO} HeLa cells treated as in (A). Data shown as means ± SEM of LTR puncta per cell or object total area per cell, minimum 500 cells were counted each well from at least 12 wells, 3 independent experiments; †, not significant (two-way ANOVA).

(C) WT or *STX16*^{KO} HeLa cells were starved in EBSS for 1 h, followed by starvation with the presence of LTR (100 nM) for additional 30 min, and subjected to HCM analysis of the colocalization between LTR and TGN46. Masks: white, cells identified based on nuclei; red, LTR puncta; green, TGN46 puncta; yellow, overlap between LTR and TGN46. Scale bar: 20 μm.

(D) Quantifications of overlaps between LysoTracker Red and TGN46 in WT and *STX16*^{KO} cells treated as in (C). Data shown as means ± SEM of LTR and TGN46 overlap area per cell, minimum 500 cells were counted each well from at least 12 wells, 3 independent experiments; **, $p < 0.01$ (two-way ANOVA).

(E) WT or *STX16/STX17*^{DKO} HeLa cells were starved in EBSS for 2 h, and subjected to ultrastructural analysis of the Golgi apparatus with electron microscopy. VF of Golgi: volume fraction of Golgi relative to total cytoplasmic area. Scale bar, 2 μm. Red arrows indicate Golgi apparatus.

Figure 7. Mammalian Atg8s regulate Stx16 localization and acidification of endolysosomal organelles

(A) WT, LC3^{TKO}, GABARAP^{TKO} or Hexa^{KO} HeLa cells were starved in EBSS for 90 min and subjected to HCM analysis of overlaps between LAMP2 and Stx16. Masks: white, cells identified based on nuclei; green, LAMP2 puncta; red, Stx16 puncta; yellow, overlap of LAMP2 and Stx16. Scale bar: 20 μm.

(B) Quantifications of overlaps between LAMP2 and Stx16 in WT, LC3^{TKO}, GABARAP^{TKO} or Hexa^{KO} HeLa cells treated as in (C). Data shown as means ± SEM of LAMP2 and Stx16 overlap area per cell, minimum 500 cells were counted each well from at least 12 wells, 3 independent experiments; *, $p < 0.05$; **, $p < 0.01$ (one-way ANOVA).

(C) Quantifications of overlaps between LBPA and Stx16 in WT, LC3^{TKO}, GABARAP^{TKO} or Hexa^{KO} HeLa cells grown in full medium or treated as in (A). Data shown as means ± SEM of LBPA and Stx16 overlap area per cell, minimum 500 cells were counted each well from at least 12 wells, 3 independent experiments; *, $p < 0.05$; **, $p < 0.01$ (one-way ANOVA). Representative images are shown in Appendix Fig. S5A.

(D) WT, LC3^{TKO}, GABARAP^{TKO} or Hexa^{KO} HeLa cells were starved in EBSS for 1 hour, followed by starvation with the presence of LTR (100 nM) for additional 30 min, and subjected to HCM analysis of LTR. Scale bar: 20 μm.

(E) Quantifications of LTR puncta in WT, LC3^{TKO}, GABARAP^{TKO} or Hexa^{KO} HeLa cells treated as in (D). Data shown as means ± SEM of LTR puncta per cell, minimum 500 cells were counted each well from at least 12 wells, 3 independent experiments; †, not significant; *, $p < 0.05$; **, $p < 0.01$ (one-way ANOVA).

(F) Schematic model of this study. Mammalian Atg8 proteins directly bind Stx16 through its LIR motif, which controls the proper localization of the Stx16 SNARE complex at the endolysosomal compartments. The Stx16 SNARE complex functions in the maintenance of lysosomal homeostasis upon autophagy induction, thus controlling mTOR activity.

Figure EV1. Peptide arrays identify a set of SNAREs bearing LIR motifs

(A) Schematics of the functional domains of SNAREs bearing LIR motifs identified through bioinformatic and peptide array analyses. LIR motifs with the amino acid sequences are marked as red bars in approximate positions on each SNARE protein. The LIR motifs in Stx16 and Stx17 are marked green as they are validated LIRs through biochemical and functional analyses.

(B) Endogenous Co-IP analysis of the interactions between LC3 and Stx16, Vti1a in HeLa and U2OS cells. * indicates IgG heavy chain of precipitated anti-LC3 antibody.

Figure EV2. Stx16 and Stx17 are required for efficient autophagic flux induced by starvation

(A) Sequences of guide RNAs (gRNA) targeting STX17 and STX16. Protospacer adjacent motif (PAM) sequences are shown in orange on the 3' side of each gRNA. The exon numbers targeted by the gRNAs are shown below each gRNA.

(B) Validation of STX16 KO, STX17 KO and STX16/STX17 DKO by Western blot analysis in HeLa and Huh7 cell lines.

(C) WT or STX17KO Huh7 cells were starved with or without the presence of bafilomycin A1 (Baf A1, 100 nM) for 2 h, and cell lysates were subjected to Western blot analysis of LC3B and p62.

(D) Quantifications of LC3B-II levels normalized to β-actin from cells treated as in (C). Data shown as means ± SEM of LC3B-II and β-actin ratios, n = 3; †, not significant (one-way ANOVA).

(E) STX16/STX17DKO HeLa cells were transfected with 3XFLAG-STX16, starved with or without the presence of Baf A1 for 2 h, and cell lysates were subjected to Western blot analysis of LC3B. Numbers below the panels are the average of LC3B-II/β-actin ratios normalized to the third lane (HeLa WT treated with EBSS plus Baf A1) from 2 independent experiments.

(F) WT or STX16/STX17DKO HeLa cells were transfected with mCherry-EYFP-GABARAP (tandem GABARAP), starved in EBSS or EBSS plus Baf A1 for 2 h, and subjected to high-content microscopic (HCM) analysis of autophagic flux for tandem GABARAP. Data shown as means ± SEM of the overlap area per cell between mCherry and EYFP, minimum 200 transfected cells were counted each well from at least 12 wells, 3 independent experiments; *, $p < 0.05$; **, $p < 0.01$ (two-way ANOVA).

(G) Representative images of tandem GABARAP transfected into WT or STX16/STX17DKO HeLa cells treated as in (F). Masks: white, cells successfully transfected with tandem GABARAP identified based on average intensity of mCherry; red, mCherry puncta in transfected cells; green, EYFP puncta in transfected cells; yellow, overlap area between mCherry and EYFP. Scale bar: 20 μm.

Figure EV3. Stx16 is required for lysosomal biogenesis

(A) Validation of STX16 and STX17 double knockout in HeLa-YFP-Parkin cells by Western blot analysis. Expression of YFP-Parkin was detected by rabbit anti-GFP antibody (ab290).

(B) Western blot analysis of LKB1 expression and AMPKα phosphorylation (Thr172) in response to H_2O_2 treatment in Huh7 cells.

(C) Western blot analysis of Stx16 and Stx17 protein levels in THP1 cells infected with lentiviruses containing STX16, STX17 or STX16 and STX17 CRISPR gRNAs.

(D) WT or STX16KO HeLa cells were starved in EBSS for 2 h and subjected to HCM analysis of the overlap between TGN46 and LAMP2. Masks: white, cells identified based on nuclei; green, TGN46 indicating trans-Golgi network (TGN); red, LAMP2 puncta; yellow, overlap between TGN46 and LAMP2. Scale bar: 20 μm.

(E) Quantifications of overlaps between TGN46 and LAMP2 in WT and STX16KO HeLa cells treated as in (A). Data shown as means ± SEM of percentages of LAMP2 overlapping with TGN46 to compensate reduced LAMP2 puncta in STX16KO cells (see Figure 5D), minimum 500 cells were counted each well from at least 12 wells, 3 independent experiments; **, $p < 0.01$ (two-way ANOVA).

(F) Co-IP analysis of the interactions between overexpressed FLAG-tagged Stx6/Stx16 and endogenous VAMP3/VAMP4/VAMP8/VPS41 in HEK293T cells under full or starved (EBSS for 1 hour) conditions.

Figure EV4. Stx16 affects lysosomal homeostasis and mTOR activity

(A) WT or STX16KO HeLa cells were starved in EBSS for 6 h and subjected to HCM analysis of the overlap between LAMP2 and mTOR. Masks: white, cells identified based on nuclei; green, LAMP2 puncta; red, mTOR puncta; yellow, overlap between LAMP2 and mTOR. Scale bar: 20 μm.

(B) Quantifications of overlaps between LAMP2 and mTOR in WT and STX16KO HeLa cells treated as in (D). Data shown as means ± SEM of overlap area per cell between LAMP2 and mTOR (upper panel), and percentages of LAMP2 overlapping with mTOR to compensate reduced LAMP2 puncta in STX16KO cells (see Figure 5D), minimum 500 cells were counted each well from at least 12 wells, 3 independent experiments; *, $p < 0.05$; **, $p < 0.01$ (two-way ANOVA).

(C) WT or STX16KO HeLa cells were starved in EBSS for 90 min, fixed and stained with GM130 and TGN46 antibodies, followed by confocal microscopy analysis of the GM130 (Golgi marker, green) and TGN46 (TGN marker, red) profiles. Scale bar, 10 μm.

(D) HCM quantifications of overlaps between GM130 and TGN46 in WT and STX16KO HeLa cells treated as in (A). Data shown as means ± SEM of overlap area per cell between GM130 and TGN46; minimum 500 cells were counted each well from at least 12 wells, 3 independent experiments; †, not significant (two-way ANOVA).

(E) WT or STX16KO HeLa cells were starved in EBSS for 90 min, fixed and stained with M6PR and TGN46 antibodies, followed by HCM analysis of the M6PR and TGN46 profiles. Masks: white, cells identified based on nuclei; green, M6PR puncta; red, TGN46; yellow, overlap between M6PR and TGN46. Scale bar: 20 μm.

(F) HCM quantifications of overlaps between M6PR and TGN46 in WT and STX16KO HeLa cells treated as in (C). Data shown as means ± SEM of overlap area per cell between M6PR and TGN46, minimum 500 cells were counted each well from at least 12 wells, 3 independent experiments; †, not significant (two-way ANOVA).

Figure EV5. mAtg8s affect acidification of the endolysosomal system and mTOR activity

(A) Western blot analysis of LC3 (LC3A,B,C), GABARAP, GABARAPL1 and GABARAPL2 in WT HeLa or cells knocked out for LC3A,B,C (LC3 TKO), GABARAP, -L1, -L2 (GBRP TKO) or all 6 mATG8s (Hexa KO).

(B) HeLa cells were transfected with WT or LIR-mutant EGFP-tagged Stx16, and subjected to HCM analysis of overlaps between Stx16 and LAMP2. Masks: white, cells transfected with Stx16 identified based on the average intensity of EGFPStx16; green, EGFP-Stx16 puncta; red, LAMP2 puncta; yellow, overlap between EGFP-Stx16 and LAMP2. Scale bar: 20 μm.

(C) HCM quantifications of overlaps between LAMP2 and WT or different types of LIRmutant EGFP-Stx16 transfected into HeLa cells and treated as in (B). Data shown as means ± SEM of percentages of EGFP-Stx16 overlapping with LAMP2, minimum 200 transfected cells were counted each well from at least 12 wells, 3 independent experiments; **, $p < 0.01$ (one-way ANOVA).

(D) Endogenous Co-IP analysis of the interactions between Stx16, Vti1a and Stx6 in WT, LC3 TKO, GABARAP TKO or Hexa KO HeLa cells. * indicates mouse IgG of precipitated mouse anti-Stx6 antibody.

(E) Endogenous Co-IP analysis of the interactions between VPS41, Stx16, Vti1a and Stx6 in WT, or ATG3 KO cells. * indicates mouse IgG of precipitated mouse anti-Stx6 antibody.

(F) WT or Hexa KO HeLa cells were starved in EBSS for indicated time points, and cell lysates were subjected to Western blot analysis of mTOR activity by mTOR substrate phosphorylation.

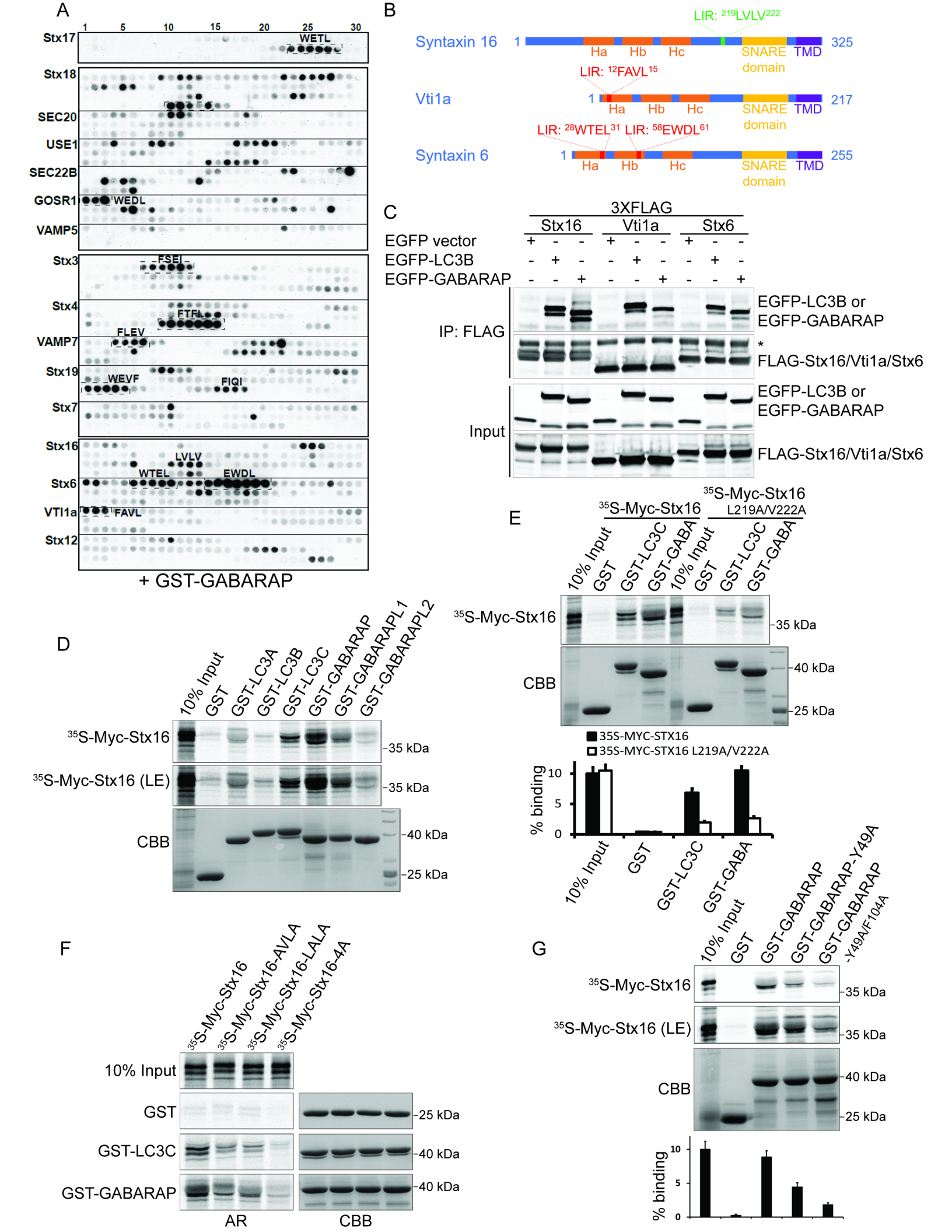
A
1 5 10 15 20 25 30
Stx17
WETL
Stx18
SEC20
USE1
SEC22B
GOSR1
WEDL
VAMP5
Stx3
FSEI
Stx4
FTRL
VAMP7
FLEV
Stx19
WEVF
FIQI
Stx7
Stx16
LVLV
WTEL
EWDL
Stx6
VTI1a
FAVL
Stx12
+ GST-GABARAP
B
Syntaxin 16
LIR: 219LVLV222
1
Ha
Hb
Hc
SNARE domain
TMD
325
Vti1a
LIR: 12FAVL15
217
Syntaxin 6
LIR: 28WTEL31
LIR: 58EWDL61
255
C
3XFLAG
Stx16
Vti1a
Stx6
EGFP vector
EGFP-LC3B
EGFP-GABARAP
IP: FLAG
EGFP-LC3B or EGFP-GABARAP
*
FLAG-Stx16/Vti1a/Stx6
Input
D
10% Input
GST
GST-LC3A
GST-LC3B
GST-LC3C
GST-GABARAP
GST-GABARAPL1
GST-GABARAPL2
35S-Myc-Stx16
35S-Myc-Stx16 (LE)
CBB
35 kDa
40 kDa
25 kDa
E
35S-Myc-Stx16
35S-Myc-Stx16 L219A/V222A
10% Input
GST
GST-LC3C
GST-GABA
35S-MYC-STX16
35S-MYC-STX16 L219A/V222A
% binding
F
35S-Myc-Stx16
35S-Myc-Stx16-AVLA
35S-Myc-Stx16-LALA
35S-Myc-Stx16-4A
10% Input
GST
GST-LC3C
GST-GABARAP
25 kDa
40 kDa
AR
CBB
G
GST-GABARAP
GST-GABARAP-Y49A
GST-GABARAP-Y49A/F104A
35S-Myc-Stx16
35S-Myc-Stx16 (LE)
CBB
35 kDa
40 kDa
25 kDa
% binding

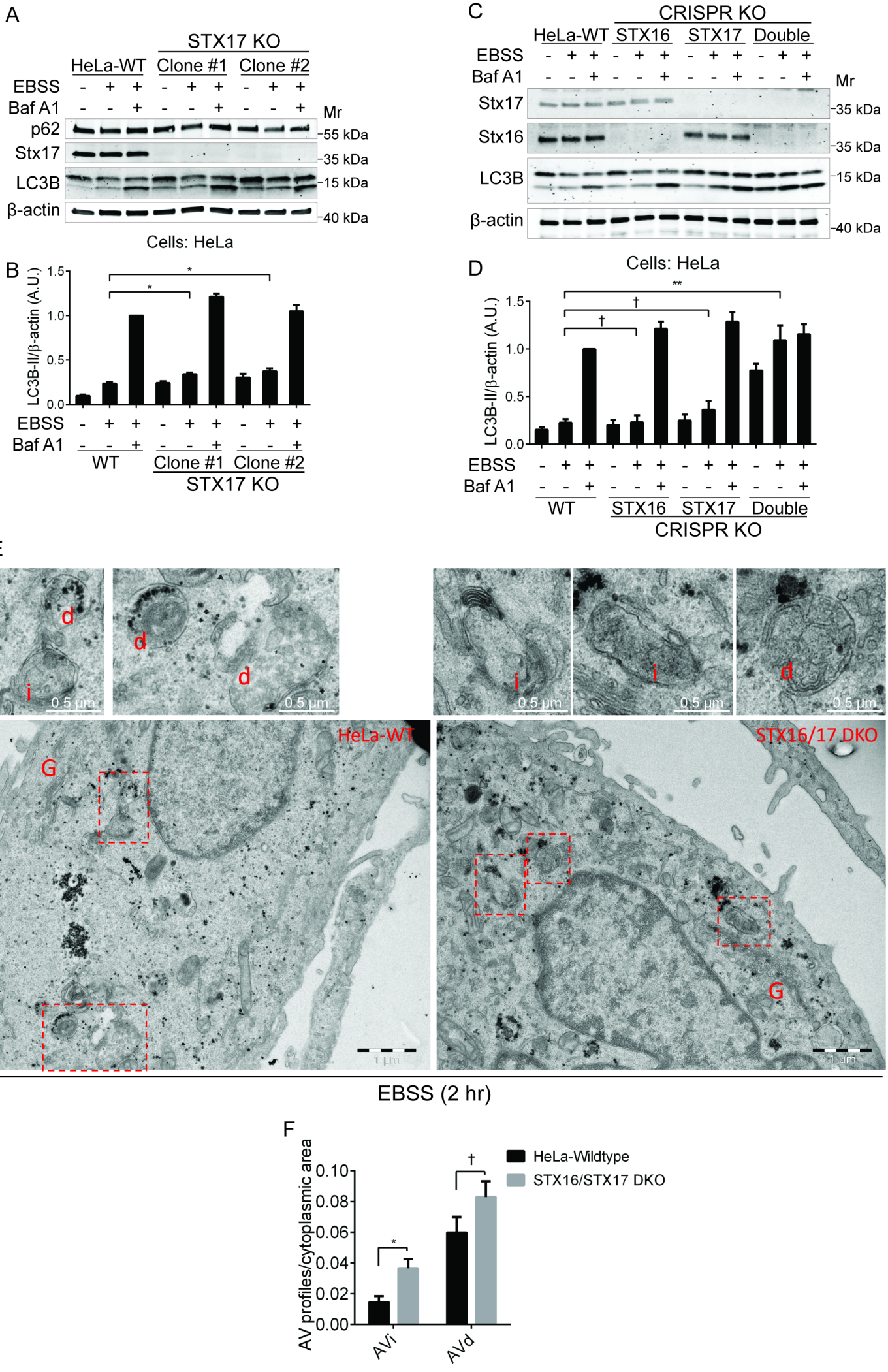
A
STX17 KO
HeLa-WT
Clone #1
Clone #2
EBSS
Baf A1
Mr
p62
Stx17
LC3B
β-actin
55 kDa
35 kDa
15 kDa
40 kDa
Cells: HeLa
B
LC3B-II/β-actin (A.U.)
WT
Clone #1
Clone #2
STX17 KO
C
CRISPR KO
HeLa-WT
STX16
STX17
Double
D
WT
STX16
STX17
Double
CRISPR KO
E
d
i
0.5 μm
HeLa-WT
STX16/17 DKO
G
1 μm
EBSS (2 hr)
F
AV profiles/cytoplasmic area
HeLa-Wildtype
STX16/STX17 DKO
AVi
AVd

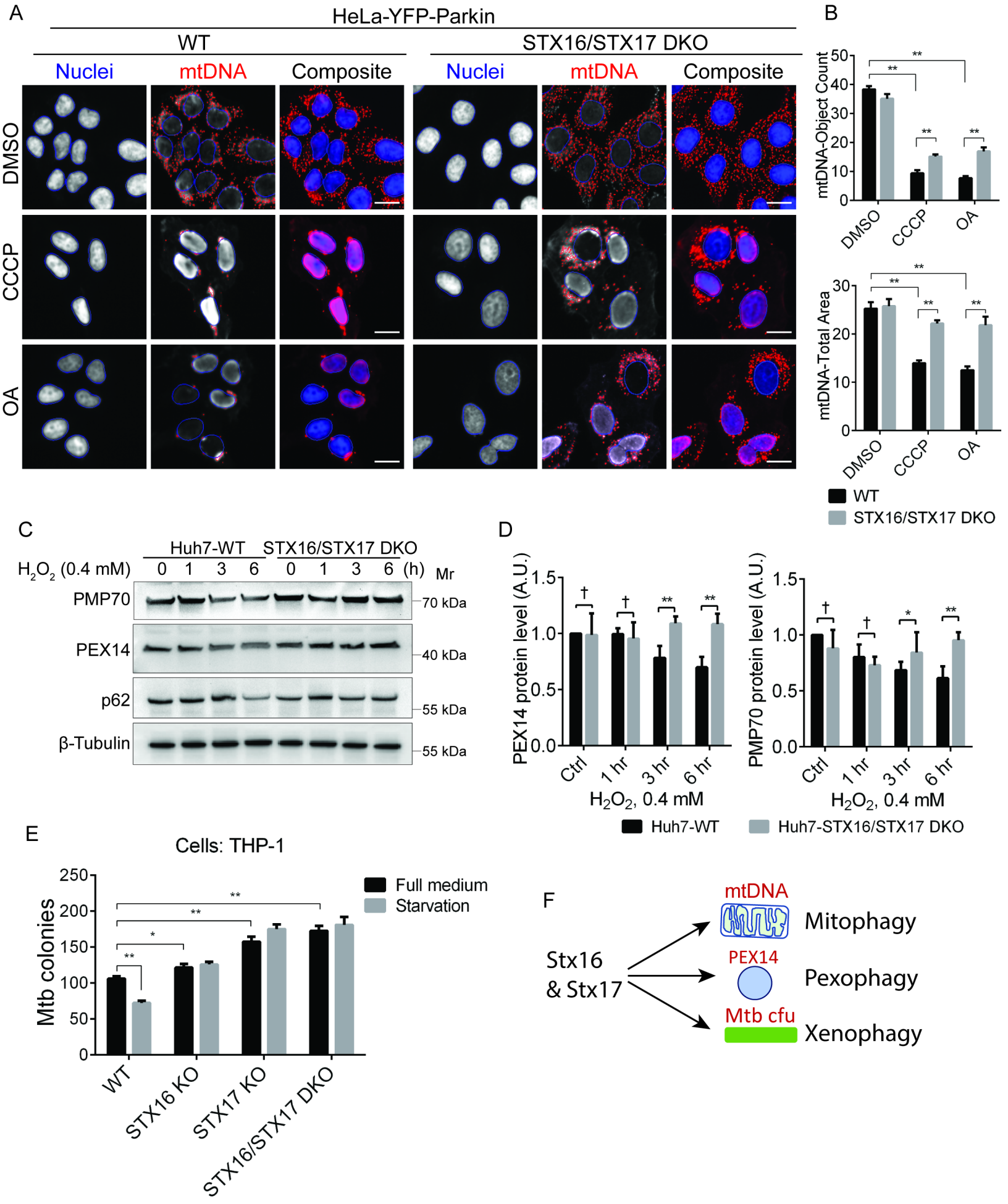
A
HeLa-YFP-Parkin
WT
STX16/STX17 DKO
Nuclei
mtDNA
Composite
DMSO
CCCP
OA
B
mtDNA-Object Count
mtDNA-Total Area
DMSO
CCCP
OA
WT
STX16/STX17 DKO
C
Huh7-WT
STX16/STX17 DKO
H2O2 (0.4 mM)
0 1 3 6 0 1 3 6 (h)
Mr
PMP70
PEX14
p62
β-Tubulin
70 kDa
40 kDa
55 kDa
55 kDa
D
PEX14 protein level (A.U.)
PMP70 protein level (A.U.)
Ctrl
1 hr
3 hr
6 hr
H2O2, 0.4 mM
Huh7-WT
Huh7-STX16/STX17 DKO
E
Cells: THP-1
Mtb colonies
Full medium
Starvation
WT
STX16 KO
STX17 KO
STX16/STX17 DKO
F
Stx16
& Stx17
mtDNA
Mitophagy
PEX14
Pexophagy
Mtb cfu
Xenophagy

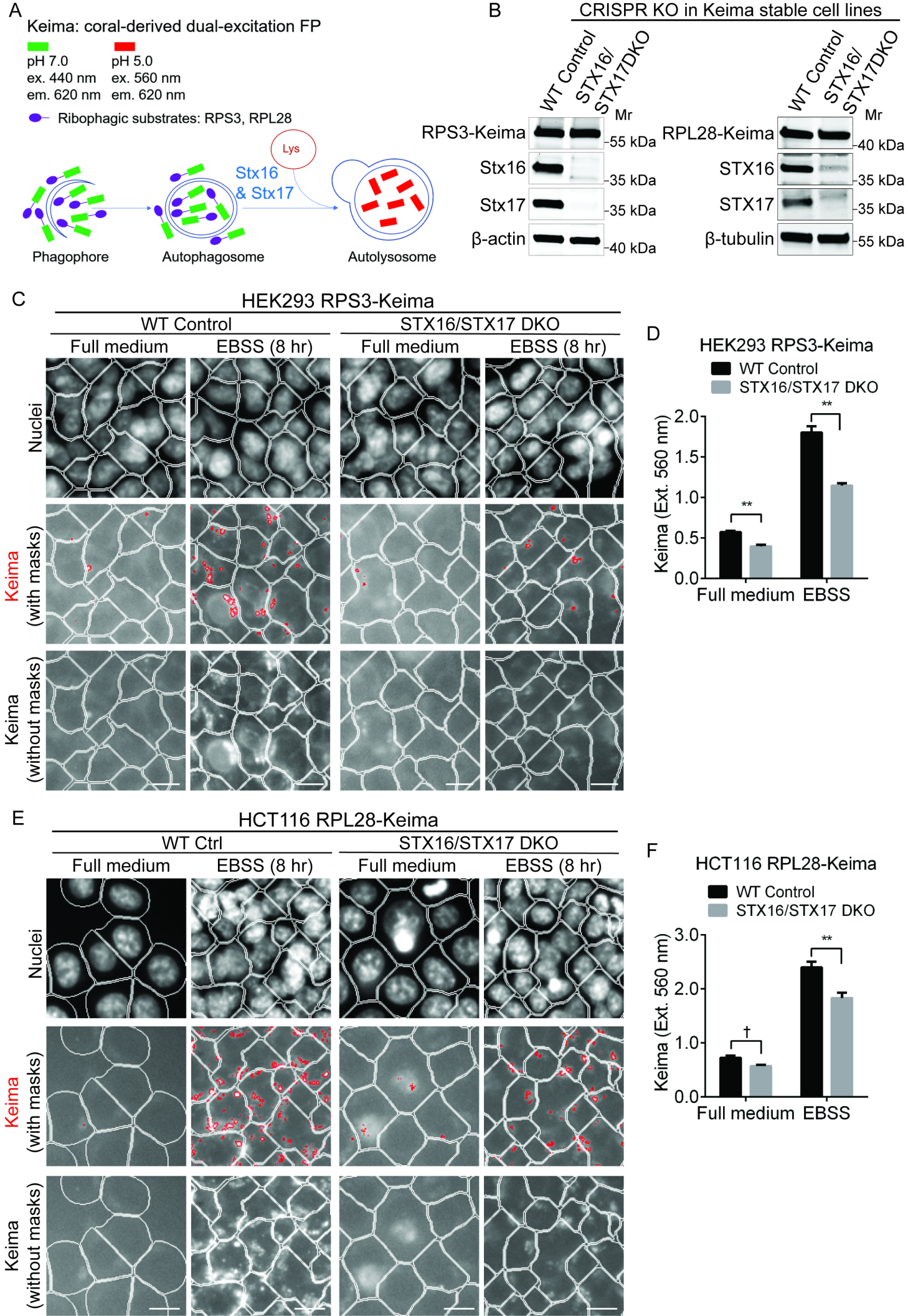
A
Keima: coral-derived dual-excitation FP
pH 7.0
ex. 440 nm
em. 620 nm
pH 5.0
ex. 560 nm
em. 620 nm
Ribophagic substrates: RPS3, RPL28
Lys
Stx16
& Stx17
Phagophore
Autophagosome
Autolysosome
B
CRISPR KO in Keima stable cell lines
WT Control
STX16/
STX17DKO
Mr
RPS3-Keima
55 kDa
Stx16
35 kDa
Stx17
35 kDa
β-actin
40 kDa
RPL28-Keima
40 kDa
STX16
35 kDa
STX17
35 kDa
β-tubulin
55 kDa
C
HEK293 RPS3-Keima
WT Control
STX16/STX17 DKO
Full medium
EBSS (8 hr)
Nuclei
Keima (with masks)
Keima (without masks)
D
HEK293 RPS3-Keima
WT Control
STX16/STX17 DKO
Keima (Ext. 560 nm)
2.0
1.5
1.0
0.5
0.0
**
**
Full medium
EBSS
E
HCT116 RPL28-Keima
WT Ctrl
STX16/STX17 DKO
Full medium
EBSS (8 hr)
Nuclei
Keima (with masks)
Keima (without masks)
F
HCT116 RPL28-Keima
WT Control
STX16/STX17 DKO
Keima (Ext. 560 nm)
3.0
2.0
1.0
0.0
**
†
Full medium
EBSS

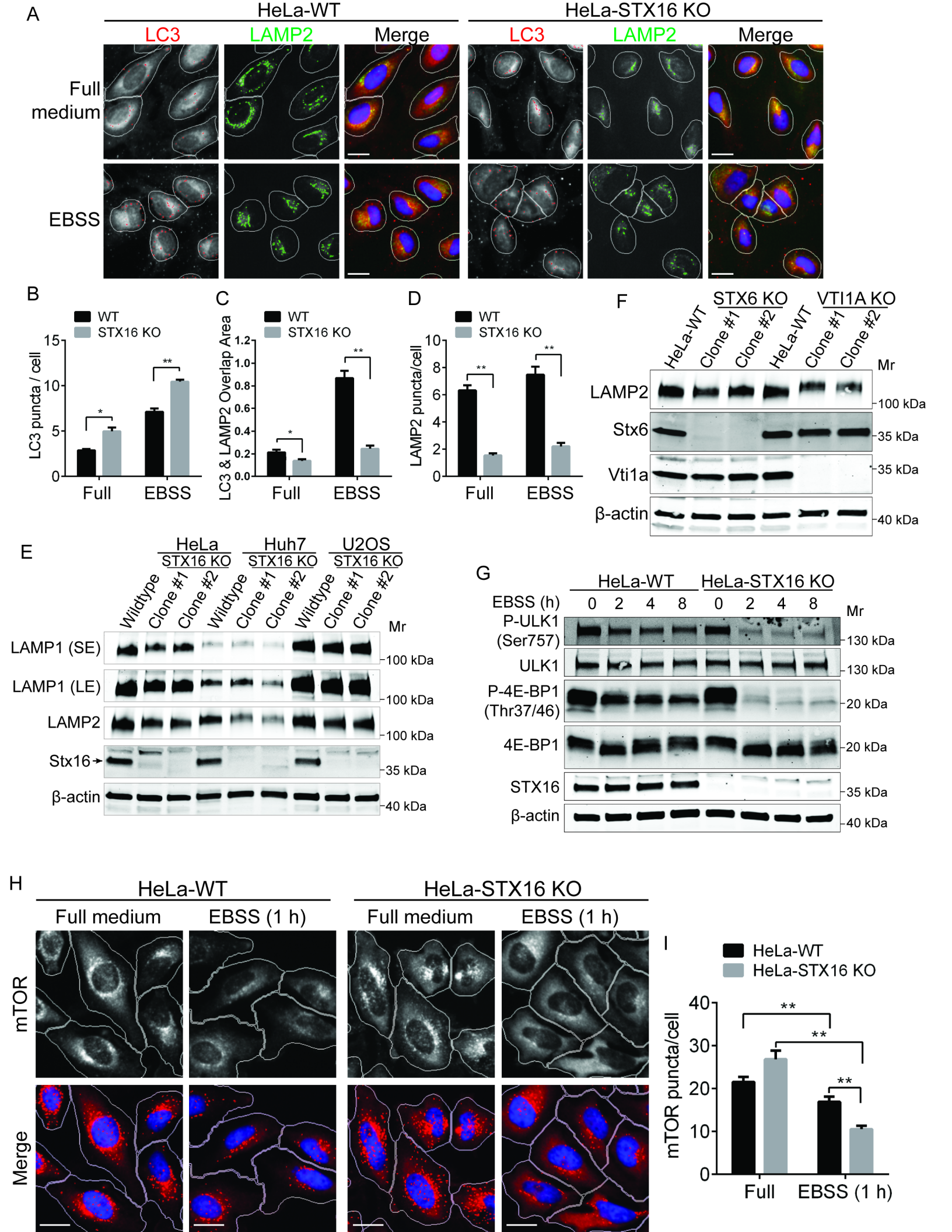
A
HeLa-WT
HeLa-STX16 KO
LC3
LAMP2
Merge
Full medium
EBSS
B
WT
STX16 KO
LC3 puncta / cell
Full
EBSS
C
LC3 & LAMP2 Overlap Area
D
LAMP2 puncta/cell
E
HeLa
Huh7
U2OS
STX16 KO
Wildtype
Clone #1
Clone #2
Mr
LAMP1 (SE)
LAMP1 (LE)
LAMP2
Stx16
β-actin
100 kDa
35 kDa
40 kDa
F
STX6 KO
VTI1A KO
Stx6
Vti1a
G
EBSS (h)
P-ULK1 (Ser757)
ULK1
P-4E-BP1 (Thr37/46)
4E-BP1
STX16
130 kDa
20 kDa
H
mTOR
Merge
I
mTOR puncta/cell

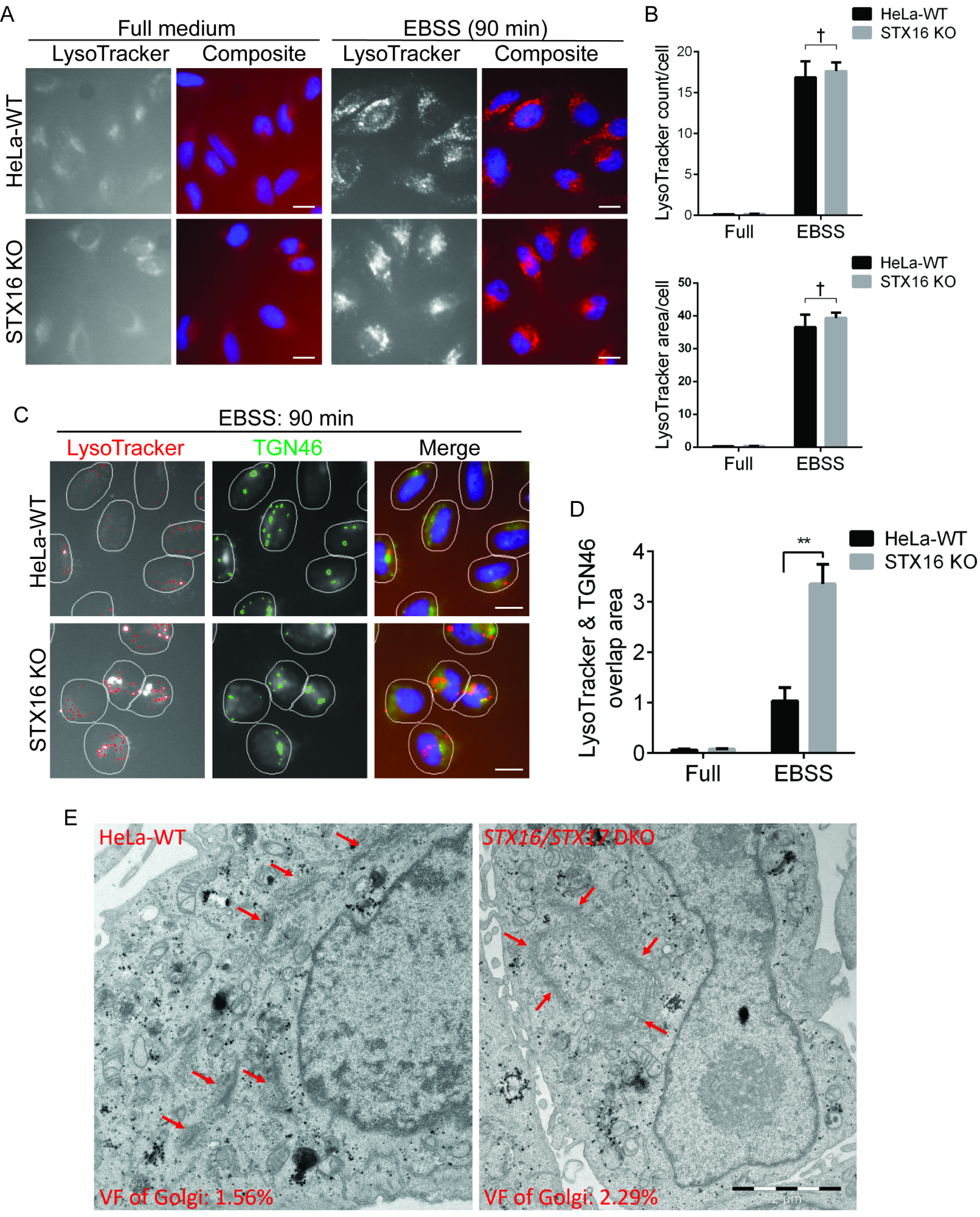
A
Full medium
EBSS (90 min)
LysoTracker
Composite
LysoTracker
Composite
HeLa-WT
STX16 KO
B
HeLa-WT
STX16 KO
LysoTracker count/cell
20
15
10
5
0
†
Full
EBSS
HeLa-WT
STX16 KO
LysoTracker area/cell
50
40
30
20
10
0
†
Full
EBSS
C
EBSS: 90 min
LysoTracker
TGN46
Merge
HeLa-WT
STX16 KO
D
HeLa-WT
STX16 KO
LysoTracker & TGN46 overlap area
4
3
2
1
0
**
Full
EBSS
E
HeLa-WT
STX16/STX17 DKO
VF of Golgi: 1.56%
VF of Golgi: 2.29%
2 μm

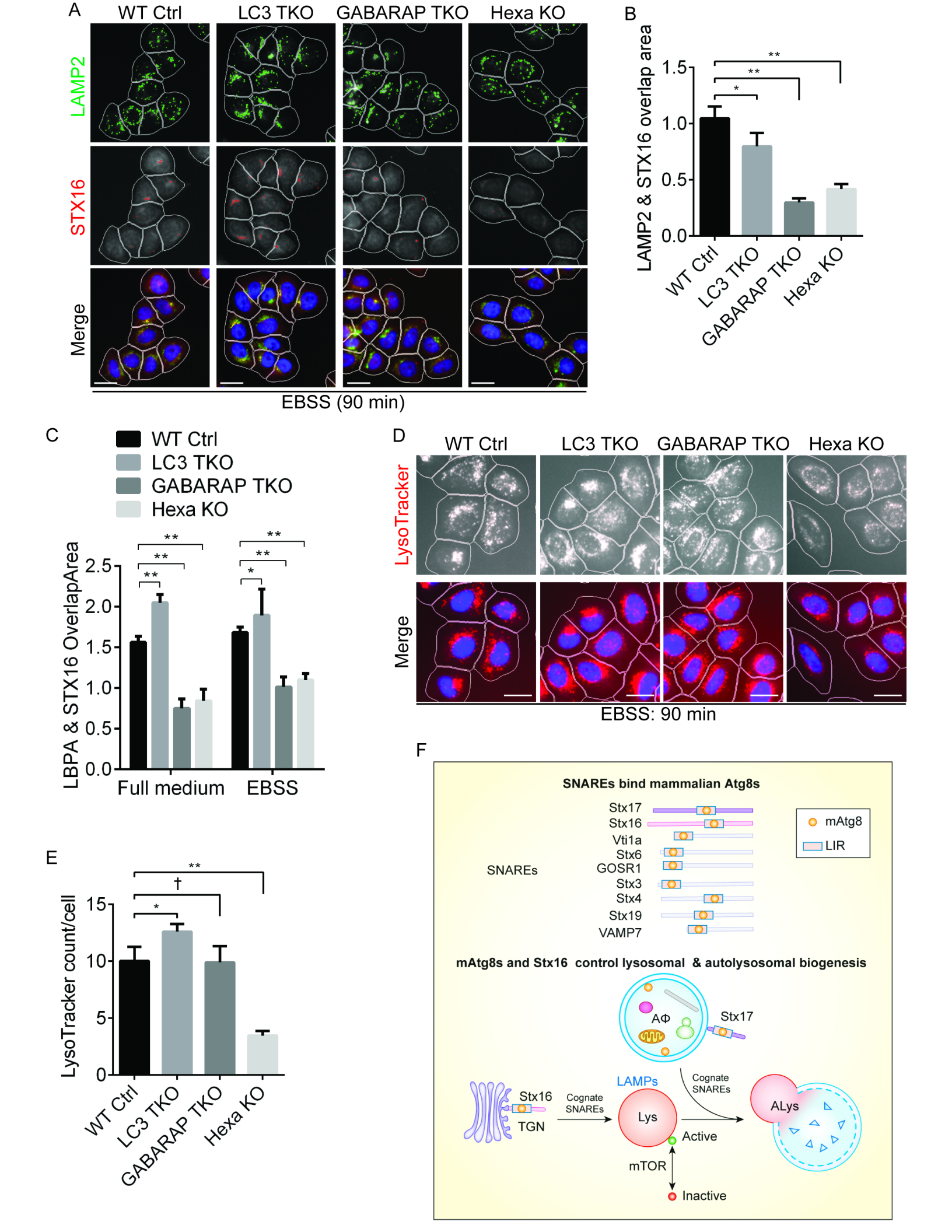
A
WT Ctrl
LC3 TKO
GABARAP TKO
Hexa KO
LAMP2
STX16
Merge
EBSS (90 min)
B
LAMP2 & STX16 overlap area
1.5
1.0
0.5
0.0
**
**
*
WT Ctrl
LC3 TKO
GABARAP TKO
Hexa KO
C
WT Ctrl
LC3 TKO
GABARAP TKO
Hexa KO
LBPA & STX16 OverlapArea
2.5
2.0
1.5
1.0
0.5
0.0
Full medium
EBSS
D
WT Ctrl
LC3 TKO
GABARAP TKO
Hexa KO
LysoTracker
Merge
EBSS: 90 min
E
LysoTracker count/cell
15
10
5
0
**
†
*
WT Ctrl
LC3 TKO
GABARAP TKO
Hexa KO
F
SNAREs bind mammalian Atg8s
SNAREs
Stx17
Stx16
Vti1a
Stx6
GOSR1
Stx3
Stx4
Stx19
VAMP7
mAtg8
LIR
mAtg8s and Stx16 control lysosomal & autolysosomal biogenesis
AΦ
Stx17
Stx16
TGN
Cognate SNAREs
LAMPs
Lys
Active
mTOR
Inactive
Cognate SNAREs
ALys